An fMRI-based brain marker of individual differences in delay discounting

Leonie Koban, Sangil Lee, Daniela Schelski, Marie-Christine Simon, Caryn Lerman, Bernd Weber, Joseph Kable, Hilke Plassmann

An fMRI-based brain marker of individual differences in delay discounting

Leonie Koban[1,2,3,*], Sangil Lee[4], Daniela S. Schelski[5,6], Marie-Christine Simon[7], Caryn Lerman[8], Bernd Weber[5,6], Joseph W. Kable[4], & Hilke Plassmann[1,2]

[1] Marketing Area, INSEAD, Fontainebleau, France
[2] Control-Interoception-Attention Team, Paris Brain Institute (ICM), INSERM U 1127, CNRS UMR 7225, Sorbonne University, Paris, France
[3] Université Claude Bernard Lyon 1, CNRS, INSERM, Centre de Recherche en Neurosciences de Lyon CRNL U1028 UMR5292, Bron, France
[4] Department of Psychology, University of Pennsylvania, Philadelphia, PA, USA
[5] Center for Economics and Neuroscience, University of Bonn, Bonn, Germany
[6] Institute of Experimental Epileptology and Cognition Research, University of Bonn Medical Center, Bonn, Germany
[7] Institute for Nutrition and Food Science, Nutrition and Microbiota, University of Bonn, Bonn, Germany
[8] Norris Comprehensive Cancer Center, University of Southern California, Los Angeles, CA, USA

*Correspondence to: leonie.koban@cnrs.fr

Abbreviated title: A BRAIN SIGNATURE OF DELAY DISCOUNTING

Financial interests or conflict of interest

The authors declare no financial interests or conflict of interests.

Acknowledgments

We received funding from the ANR (Tremplin-ERC grant “Brain Gut Decision” to HP), Campus France (Marie-Sklodowska-Curie co-fund fellowship PRESTIGE-2018-2-0023 to LK), French federal funding (program ‘Investissements d’avenir’, ANR-10-IAIHU-06), the Federal Ministry of Education and Research Germany (Diet-Body-Brain grant 01EA1809B to BW and 01EA1707 to MCS), the National Cancer Institute (R35CA197461 [CL] and R01CA170297 [JK and CL]), and the AE Foundation (to JK). The funders had no role in study design, data collection and analysis, decision to publish, or preparation of the manuscript. We thank P. Trautner for help with the programming of the task (Study 1); A. Simonetti, M. Boerth, J. Tholen, A.-A. Ortner, A. Koehlmoos, S. Winkler, L. Bernardo, A. M. Burke, M. K. Caulfield, N. Cooper, G. Donnay, M. Falcone, J. Jorgensen, R. Kazinka, J. Luery, M. McConnell, R. Miglin, D. Mukherjee, T. Parthasarathi, S. Price, M. Schlussel, R. Sharp, H. J. Sohn, D. Spence, and K. Terilli for help with data acquisition; and T. D. Wager for the Canlab toolbox and helpful discussion.

Abstract

Individual differences in delay discounting—how much we discount future compared to immediate rewards—are associated with general life outcomes, psychopathology, and obesity. Here, we use machine learning on fMRI activity during an intertemporal choice task to develop a functional brain marker of these individual differences in human adults. Training and cross-validating the marker in one data set (Study 1, N = 110 male adults) resulted in a significant prediction-outcome correlation (r = 0.49), generalized to predict individual differences in a completely independent data set (Study 2, N = 145 male and female adults, r = 0.45), and predicted discounting several weeks later. Out-of-sample responses of the functional brain marker, but not discounting behavior itself, differed significantly between overweight and lean individuals in both studies, and predicted fasting state blood levels of insulin, c-peptide, and leptin in Study 1. Significant predictive weights of the marker were found in cingulate, insula, and frontoparietal areas, among others, suggesting an interplay among regions associated with valuation, conflict processing, and cognitive control. This new functional brain marker is a step towards a generalizable brain model of individual differences in delay discounting. Future studies can evaluate it as a potential transdiagnostic marker of altered decision-making in different clinical and developmental populations.

Significance statement

People differ substantially in how much they prefer smaller sooner or larger later rewards such as spending money now versus saving it for retirement. These individual differences are generally stable over time and have been related to differences in mental and bodily health. What is their neurobiological basis? We applied machine-learning to brain imaging data to identify a novel brain activity pattern that accurately predicts how much people prefer sooner versus later rewards, and which can be used as a new brain-based measure of intertemporal decision-making in future studies. The resulting functional brain marker also predicts overweight and metabolism-related blood markers, providing new insight into the possible links between metabolism and the cognitive and brain processes involved in intertemporal decision-making.

Introduction

Many decisions in life have consequences at different points in time. For example, most people need to decide whether to put part of their paycheck towards a retirement fund or spend it on something fun, like a short vacation. These trade-offs between options that are immediately rewarding and those that will be more rewarding in the long run are hard, and people differ substantially in *delay discounting*—the degree to which they discount future compared to immediate rewards (Kirby and Herrnstein, 1995). Greater delay discounting (i.e., greater impatience or higher preference for sooner rewards) is associated with obesity, addiction, and many psychiatric conditions (Bickel et al., 1999; MacKillop et al., 2011; Mole et al., 2015; Amlung et al., 2016). It has therefore been proposed as a potential transdiagnostic marker of psychopathology (Amlung et al., 2019; Lempert et al., 2019) and as a risk factor for short-sighted behaviors such as unhealthy diet, smoking, and excessive alcohol and drug use (Audrain-McGovern et al., 2009; Fernie et al., 2013). The goal of the present study is to identify and validate an fMRI-based brain marker of individual differences in delay discounting.

Previous findings regarding the structural and functional brain bases of individual differences in delay discounting offer a mixed picture. Several studies suggest a role for areas involved in reward processing and valuation (Bartra et al., 2013; Cooper et al., 2013), and for areas central to cognitive control (Hare et al., 2014). Brain areas associated with memory and prospection have also been found to contribute to individual differences in delay discounting (Benoit et al., 2011; Peters and Büchel, 2011; Lebreton et al., 2013). Studies using structural and functional connectivity measures suggested a role for fronto-striatal and striatal-subcortical connections (van den Bos et al., 2014). The structure of midbrain dopaminergic nuclei and the ventral striatum has been associated with self-reported trait impulsivity (MacNiven et al., 2020).

Individual differences in delay discounting may also emerge from the combined activity across multiple brain regions or functional networks. However, only a few studies (Berman et al., 2013; Li et al., 2013; Pehlivanova et al., 2018) have investigated the distributed patterns associated with individual differences in delay discounting. Further, most previous studies used relatively small sample sizes to explore these individual differences, increasing the risk of both false-positive and false-negative results (Poldrack et al., 2017). Given the use of standard correlation or regression analyses that are typically not cross-validated on independent data samples, previous results are difficult to compare with each other and do not provide any formal model that could predict delay discounting in completely independent studies.

Here, we address these limitations by using a machine-learning-based 'brain model' approach (Woo et al., 2017; Kragel et al., 2018). Brain models are trained to predict a mental process or individual variable (here, delay discounting) and can be applied to independent data (Kragel et al., 2018; Scheinost et al., 2019). As such, brain models go beyond reporting peak coordinates by identifying specific large-scale patterns of brain activity that can be replicated, validated, or falsified in a quantifiable way. This approach has been successfully applied to brain-based prediction of pain (Wager et al., 2013), working memory (Rosenberg et al., 2020), and affective states (Yu et al., 2020), among others. The importance of independent validation and model generalizability has also been recognized for brain-based prediction of trait-like individual differences (Gabrieli et al., 2015; Rosenberg et al., 2018; Rosenberg and Finn, 2022).

Here, we build on this approach to predict individual differences in delay discounting. If there is a consistent activity pattern associated with individual differences in delay discounting during intertemporal choices, then this pattern should be able to predict delay discounting in new data (hold-out subjects) and even completely independent data sets. Comparing the resulting pattern to meta-analysis-based masks

allows us to assess the contribution of brain areas associated with valuation, cognitive control, and prospection.

Materials and methods

Overview

We used an established machine-learning algorithm, LASSO-PCR (Tibshirani, 1996; Wager et al., 2011) and fMRI data from two independent studies, from different scanners, labs, and countries. Study 1 (N=110) was used for training and cross-validation of a predictive model of individual differences in delay discounting. Study 2 (existing data set from previously published study, see Kable et al., 2017, N=145) was used as an independent test data set to assess the validity and replicability of the predictive model.

Participants

For Study 1, participants were recruited in the context of a seven-week dietary intervention study at the University of Bonn in Germany (https://osf.io/rj8sw/?view_only=af9cba7f84064e61b29757f768a8d3bf). Due to the nature of this longitudinal intervention study, we recruited only male participants who further fulfilled the following inclusion criteria: age between 20 and 60 years, right-handedness, non-smoker, no excessive drug or alcohol use in the past year, no psychiatric or neurological disease, body mass index (BMI) between 20 and 34, no other chronic illness or medication, following a typical Western diet without dietary restrictions, and no MRI exclusion criteria (large tattoos, non-removable piercings, metal in the body, claustrophobia, etc.). N=116 male participants performed the intertemporal choice task in Study 1. Here, we focus on behavioral and fMRI data collected during a baseline session before the group assignment and dietary intervention (to be reported elsewhere) and use post-intervention behavioral data only for demonstrating the temporal stability of

interindividual differences in delay discounting. The data of six participants had to be excluded for analysis due to the following reasons: technical problems with the scanner (1), with the synchronization between stimulation software and scanner (3), and with the response box (1), and strong motion artifacts (>5mm) and participant quitting the task mid-scan (1). Therefore, 110 participants (mean age=31.7; 52 lean, 48 overweight, and 10 obese; BMIs ranging from 20.6 to 33.7) were included in the final analysis of Study 1. There were no significant differences between lean and overweight-to-obese participants in age, education, or total brain volume (see Table 1). Data from 109 participants were available for the seven-week follow-up measurements (i.e., one participant did not return for the second session).

Study 2 was conducted in the context of a large cognitive training study at the University of Pennsylvania in the United States (Kable et al., 2017). The goal was to examine whether commercial cognitive training software leads to significant changes in decision-making behaviors, including delay discounting. Participants completed two sessions of scans 10 weeks apart. As with Study 1, we focus on the baseline (pre-intervention) behavioral and fMRI data, and report post-intervention behavioral data only to assess the temporal (10-week) stability of interindividual differences in delay discounting. Of the 160 non-pilot participants who completed session 1, we excluded those with missing runs (N=6), frequent or significant head movement (any run with >5% of mean image displacements greater than 0.5mm; N=3), more than 3 missing trials per run for two or more runs (N=2), or lack of participant blinding (N=1, one subject expressed awareness of their experimental condition, i.e. cognitive training vs. control). Of the remaining 148, we excluded three more participants whose choice was entirely one-sided (i.e., choosing only immediate reward or delayed reward), resulting in a final sample of N=145 participants for Study 2 (88 male, 57 female, mean age=24.4; 81 lean, 39 overweight, and 25 obese; BMIs ranging from 16.5 to 40.9). There were no significant

differences between lean and overweight-to-obese participants in sex, age, education, or total brain volume (see Table 1). Due to drop-out, data from 102 participants was available for the 10-week post-intervention measurement of log(k).

The study protocols were approved by the institutional review boards of Bonn University's Medical School (Study 1) and the University of Pennsylvania (Study 2). All participants provided written informed consent, and were paid for their time and participation in the study. The research reported here complies with all relevant ethical regulations.

Stimuli and task

In Study 1, participants performed 108 choices (trials) between varying amounts of smaller sooner (SS) and larger later (LL) options, presented on the left or right of the screen (position randomized; see Figure 1a). Participants were instructed that one of their choices might be paid out at the end of the experiment. Thus, participants' choices were non-hypothetical and incentive-compatible. During each trial, the two options were presented for 4s, during which participants could make their choice (left or right) by pressing the corresponding response key with their left or right index finger, respectively. Once the choice had been made, a yellow frame highlighted the chosen option and remained on the screen for the remainder of the 4s. Intertrial intervals were jittered using an approximately geometric distribution (2–11s)

SS options varied among €5, €10, and €20, and always had zero delay ('today'). LL options varied between €5 and €96.80 and had delays between 2 days and 8 months (~240 days, choice combinations are presented in Figure 1-1). Amounts and delays were chosen to allow fine-grained estimation of individual k's between 0 and 0.256. Trials were presented in randomized order.

The intertemporal choice task in Study 2 consisted of 120 trials, again with the same choice sets for all participants (see Figure 1-2). In contrast to Study 1, the SS amount was fixed at US$20. Thus, participants were presented with the LL option (with amount ranging from US$22 to US$85 and delays from 19 days to 180 days) and were instructed to press one of two keys to either accept and receive this LL offer, or to reject the LL offer and receive the SS offer ($20 today) instead. Participants were informed that one trial would be randomly chosen at the end of the experiment and their choices implemented (i.e., the chosen amount would be paid via wire transfer at the indicated time delay), resulting in incentive-compatible and mutually independent choices in each trial (as in Study 1).

Blood measures and body fat measures

In Study 1, blood samples in a fasted state were collected from participants' non-dominant arm before they received a standardized breakfast. HOMA-IR (a marker of insulin resistance) was calculated as the product of fasting insulin and glucose levels, divided by 405 (Lozano et al., 2012). Body weight and proportion of body fat were measured using a bioimpedance scale (Tanita Europe BV, Amsterdam, the Netherlands). For technical reasons, this body fat measure was available for only 103 participants.

Experimental design and statistical analyses

Behavioral measures. For each participant, we calculated the proportion of SS choices (with respect to total number of non-misses) and the model-based discounting parameter k. Individual k's were log-transformed in both studies to obtain less skewed distributions of discounting parameters. This log(k)-parameter describes the steepness of discounting as modeled by the hyperbolic discounting function (Kirby and Herrnstein, 1995). Higher log(k) parameters reflect steeper discounting and thus greater impatience;

smaller (more negative) values reflect less steep discounting and thus more patient decision-making.

In Study 1 we computed k by calculating the proportion of SS choices for all target k's (i.e., the k-value for which SS and LL options of any given choice trial should theoretically be chosen at 50% each). We then used linear interpolation to identify the individual indifference point at which the proportion of SS and LL choices was equal (50% each).

In Study 2, we fit a logit utility model on choice data via maximum likelihood estimation. The logit of the probability of choosing the delayed reward was modeled as follows:

$$\mathrm{logit}\big(\mathrm{p}(\mathrm{Y_t} = \mathrm{delayed})\big) = \sigma\left(\frac{\mathrm{LL_t}}{1 + \mathrm{kD_t}} - 20\right)$$

Where LL_t is the LL amount in trial t and D_t is the delay in trial t. σ was included as a scaling parameter that controls the relationship between utility difference scale and choice.

MRI data acquisition. Functional and structural brain imaging data for Study 1 were acquired using a Siemens Trio 3T scanner (Erlangen, Germany) at the Life & Brain Institute, Bonn University Hospital, Germany. Functional images used a T2* weighted EPI-GRAPPA sequence (TR=2.5s, TE=30ms, flip angle=90°, FOV=192mm, acceleration factor R=2, average of 400 volumes) and covered the whole brain in 37 slices (voxel size of 2 x 2 x 3mm, 10% interslice distance). Structural images were acquired using a T1 weighted MPRAGE sequence (1mm isomorphic voxels).

For Study 2, the functional and structural imaging data were acquired with a Siemens 3T Trio scanner with a 32-channel head coil. High-resolution T1-weighted anatomical images were acquired using an MPRAGE sequence (T1=1100ms; 160 axial

slices, 0.9375 x 0.9375 x 1.000mm; 192 x 256 matrix). T2*-weighted functional images were acquired using an EPI sequence with 3mm isotropic voxels, 64 x 64 matrix, TR=3s, TE=25ms, 53 axial slices (no interslice gaps), 104 volumes. B0 fieldmap images were collected for distortion correction (TR=1270ms, TE=5 and 7.46ms).

Preprocessing and basic statistical analyses of fMRI data. Preprocessing for Study 1 was performed in SPM12 and used a standard pipeline of motion correction, slice time correction, spatial normalization to MNI space, and spatial smoothing of images using an 8mm FWHM Gaussian kernel. Preprocessing for Study 2 was performed in FSL according to the original preprocessing pipeline (Kable et al., 2017). This involved the standard pipeline of motion correction, b0 map unwarping, interleaved slice time correction, spatial smoothing with FWHM 9mm Gaussian kernel, and high-pass filtering (cutoff=104s).

For Study 1, we used SPM12 to fit a general linear model (GLM) for each participant's imaging data, with choice screen onset modeled as a stick function (0s duration) as the main regressor and mean-centered parametric modulators for delay, relative LL amount (LL amount divided by SS amount), SS amount, and reaction time. Six nuisance regressors were added to control for movement artifacts. For Study 2, FSL was used to fit an otherwise similar statistical model with a choice screen onset as main regressor and mean-centered parametric modulators for delay, LL amount, and reaction time. As in Study 1, six movement regressors were added to control for head movement.

Individual contrast images were calculated for the following three regressors of interest that were available for both studies: 1) choice screen onset versus implicit baseline (hereafter referred to as "Choice contrast"), 2) parametric modulation by (relative) LL amount ("LL Amount"), and 3) parametric modulation by delay ("Delay"). Contrast images were gray matter-masked to remove voxels that were unlikely to contain

meaningful BOLD signal and individually z-scored to remove differences in scale across images (and thereby make results transferable across studies and data sets).

Training and cross-validation.

Training and cross-validation were performed on data from Study 1 only (see Figure 1b). Individual differences in delay discounting may result from how participants respond to intertemporal choices overall, from how they process future rewards, and from how they process time delays. Thus, to capture a combination of functional processes that together determine delay discounting, we concatenated the contrast images for Choice, LL Amount, and Delay for each participant, resulting in a feature space that was triple the size of a single brain image. We then used LASSO-PCR (least absolute shrinkage and selection operator-principal component regression) (Tibshirani, 1996)—a machine learning-based regression algorithm—to train a classifier to predict log(k) across all voxel weights of the concatenated contrast images. LASSO-PCR first performs data reduction using principal component regression, thus identifying brain regions and networks that are highly correlated with each other. It then performs the LASSO algorithm, which shrinks regression weights towards zero, thus reducing the contribution of less important and more unstable components. LASSO-PCR has been shown to be advantageous for brain images for several reasons (see Wager et al., 2011; Wager et al., 2013): it is adequate for predictions based on thousands of voxels, it takes into account multicollinearity between voxels and brain regions, and it yields interpretable results by allowing reconstruction of voxel weight maps based on PCR results.

To assess the predictive accuracy of the classifier in new subjects, we used 10-fold cross-validation. Thus, the training data was split up in 10 stratified combinations of training (90%) and test sets (10%), such that every subject's data was used for the training of the classifier in nine folds and held out in the remaining fold to independently assess

the prediction-outcome correlation. Tenfold cross-validation was chosen *a priori* as a good compromise between maximizing the sample size in each training set and being within the range of recommended folds (between 5 and 10) (Scheinost et al., 2019; Poldrack et al., 2020). *A priori* set default regularization parameters were used for all machine-learning analysis to avoid biasing the model parameters to the data and thereby generating over-optimistic accuracy scores. Permutation tests (5,000 iterations of randomly permuting the log(k) values) were used to generate null distributions and to assess the statistical significance of the prediction-outcome correlation and the mean absolute error. Out-of-sample predictions of log(k) were used for all correlational analysis (e.g., with BMI, age, blood markers).

Bootstrapping and thresholding. To identify the brain areas contributing the most reliable positive or negative weights, we performed a bootstrap analysis; 5,000 samples with replacements were taken from the paired brain and outcome data, and the LASSO-PCR was repeated for each bootstrap sample. Two-tailed, uncorrected p-values were calculated for each voxel based on the proportion of weights above or below zero (Wager et al., 2011; Wager et al., 2013). False discovery rate (FDR) correction was applied to p-values to correct for multiple comparisons across the whole feature space (three combined brain maps).

Independent test set. Study 2 was used as an independent test set to assess the validity and generalizability of the brain pattern classifier developed based on Study 1 (i.e., the k-marker). For this purpose of testing its validity in an independent data set (and for all future use of this brain-based model), the k-marker was trained on the data of all participants of Study 1. To assess the response of the predictive marker in Study 2, we calculated the matrix dot product between the k-marker and the concatenated contrast

images (Choice screen onset, LL Amount, and Delay) from each participant. The dot product reflects the pattern similarity between the classifier and each participant's set of contrast images and, in sum with the classifier's intercepts, provides a predicted value of log(k). Predictive accuracy of the marker was quantified by correlating the predicted value of log(k) with the actual log(k)'s of each participant and by calculating the mean absolute error for each prediction.

Other statistical analyses. All statistical tests were performed in Matlab, were two-tailed, and used a significance criterion of p=0.05. Statistical power calculations confirmed that the sample sizes in both studies were sufficiently powered (>80%) to detect correlations of $r > 0.3$ at a significance level of p=0.05 (two-sided tests).

Results

Individual differences in delay discounting

In Study 1 (Bonn University, N=110), participants chose the SS option in an average of 43.7% of all trials (median=48.1%) and had a fitted mean log(k) parameter of -5.70 (median log(k)=-5.28, corresponding to a k of 0.0051). Choice behavior was characterized by substantial individual differences, with %SS choices ranging from 5.6% to 88.8%, and log(k) ranging from -9.90 to -1.36 (see Figure 1c). Individual differences were very stable over a 7-week period (see Methods), with a test-retest reliability (correlation between baseline log(k)'s and second session) of r=0.86 (p<0.001, 95%-confidence interval [CI]=[0.80, 0.90], Figure 1c).

On average, participants in Study 2 chose the SS option in 57.4% of trials (median=60.0%) and had an fitted log(k) of -4.08 (median log(k)=-3.95, corresponding to a k of 0.0193). Again, individuals varied substantially in their intertemporal preferences, with %SS ranging from 0.8% to 99.2%, and log(k) ranging from -7.08 to -2.12 (see Figure

1c). As in Study 1, these individual differences were stable over time, with a test-retest reliability between baseline and post-intervention (10 weeks later) measures of log(k) of r=0.74 (Pearson correlation, p<0.001, 95%-CI=[0.63, 0.82], see Figure 1c). Thus, our data confirm both the substantial variability in delay discounting known from previous work (Kable and Glimcher, 2007; Pehlivanova et al., 2018) and the stability of these individual differences over time (Kirby, 2009; Anokhin et al., 2015; Lempert and Phelps, 2016), allowing us to investigate the neurofunctional bases of these individual differences.

Significant cross-validated prediction of delay discounting based on fMRI

Training (using LASSO-PCR) and cross-validating (10-fold) the predictive marker (termed k-marker, see Figure 2a) in Study 1 resulted in a cross-validated prediction-outcome correlation (i.e., correlation between predicted and actual log(k)) of r=0.49 (permutation test: p<0.001), a mean squared error of 2.84 (permutation test: p<0.001), and a mean absolute error for predicted log(k) of 1.32 (permutation test: p<0.001; see Figure 2b-c for additional results and random cross-validation folds). The explained variance of the prediction compared to a hypothetical mean model (prediction R^2) was R^2=0.23. Individual differences in head motion (mean absolute framewise displacement) were neither related to log(k) (Pearson correlation: r=-0.05, p=0.58) nor predicted log(k) (Pearson correlation: r=0.01, p=0.92). Statistically controlling for age, education, head motion, and total brain volume (using partial correlations), did not substantially change the relationships between actual log(k) and predicted log(k) (Partial correlation: r=0.54, p<0.001). Out-of-sample k-marker responses also predicted percentage of SS choices (Pearson correlation: r=0.50, p<0.001) and log(k) calculated based on the method of Study 2 (Pearson correlation: r=0.45, p<0.001).

Validation of the k-marker in an independent test data set (Study 2)

Brain markers of individual differences become more meaningful if they can be validated in different and completely independent data (Kragel et al., 2018). The validity of the marker should not depend on study-specific parameters such as the type of scanner used for data acquisition, preprocessing software, or other aspects of the data (Woo et al., 2017; Kragel et al., 2018; Scheinost et al., 2019).

We therefore tested whether the k-marker—developed and cross-validated entirely on Study 1—could predict discounting in a completely independent data set. The validation data set (Study 2) was acquired on a different scanner, in a different lab and country, and using a different participant sample and different task characteristics, and was preprocessed and analyzed using different MRI analysis software. Evaluating the performance of the k-marker in Study 2 is therefore an even stronger test than cross-validation in Study 1 alone.

For this purpose, we computed the pattern expression of the k-marker using the matrix dot product for each participant's data (contrast images for Choice, parametric modulation for LL Amount, and Delay) in Study 2. The resulting predicted log(k) values were significantly correlated with actual log(k) values (Figure 2c), Pearson correlation: $r=0.45$, $p<0.001$, 95%-CI=[0.31, 0.57], mean absolute error of 1.68) demonstrating the replicability of the k-marker in a completely independent data set. For the transfer test to Study 2, prediction R^2 was -3.2, indicating that, while the k-marker was very accurate in identifying the rankings among individuals, the absolute prediction values were less accurate than a hypothetical mean model.

The training and cross-validation data set (Study 1) consisted of male participants only, which might limit the validity of the k-marker in females. We therefore assessed the accuracy of the k-marker in Study 2 separately in male and female participants (see Figure 2c). In male participants (N=88), the prediction-outcome correlation was $r=0.40$ (Pearson correlation: $p<0.001$, 95%-CI=[0.21, 0.56]). In females (N=57), the prediction-outcome

correlation was r=0.55 (Pearson correlation: p<0.001, 95%-CI=[0.34, 0.71]) and thus comparable, if not superior, to the predictive accuracy in males. This demonstrates that the k-marker (despite being trained on male participants' data only) predicts delay discounting well for both male and female participants. As in Study 1, individual differences in head motion in Study 2 were neither related to log(k) (Pearson correlation: r=0.12, p=0.14) nor predicted log(k) (Pearson correlation: r=0.04, p=0.59). Statistically controlling for age, sex, education, head motion, and total brain volume did not change the relationship between predicted and actual log(k) (Partial correlation: r=0.44, p<0.001, 95%-CI=[0.30, 0.56]).

Brain-based prediction of future discounting

We next assessed whether responses of the k-marker were predictive of individual differences in delay discounting as measured several weeks later. Responses of the k-marker at baseline significantly predicted (out-of-sample) discounting behavior seven weeks later in Study 1 (Pearson correlation: r=0.38, p<0.001, 95%-CI=[0.20, 0.53]) and 10 weeks later in Study 2 (Pearson correlation: r=0.36, p=0.002, 95%-CI=[0.17, 0.51]; see Figure 2d). This shows that variability in k-marker responses is driven largely by stable individual differences and their underlying neurophysiological processes.

Response of the k-marker differs between lean and overweight participants

Given previous findings of higher delay discounting in overweight and obese people (Jarmolowicz et al., 2014; Amlung et al., 2016), we next tested whether individual differences in k-marker response were associated with individual differences in body mass and overweight (as measured by the body mass index [BMI] > 25). In contrast to previous reports (MacKillop et al., 2011; Amlung et al., 2016) that have studied this relationship more systematically, actual log(k) was not significantly correlated with BMI in either of the

two samples (Pearson correlations: Study 1: r=0.07, p=0.48, 95%-CI=[-0.12, 0.25]; Study 2: r=-0.04, p=0.69, 95%-CI=[-0.20, 0.12]). However, in Study 1, response of the k-marker significantly correlated with both BMI (Pearson correlation: r=0.26, p=0.005, 95%-CI=[0.08, 0.43]; see Figure 3a) and percentage of body fat (Pearson correlation: r=0.28, p=0.004, 95%-CI=[0.09, 0.45]). The k-marker response in Study 1 also differed between lean (BMI <= 25) and overweight-to-obese (BMI > 25) participants (two-sample t-test: t(108)=2.85, p=0.005, Cohen's d=0.55, 95%-CI=[0.12, 0.69]; see Figure 3b). Further, k-marker response in Study 1 significantly predicted metabolic blood markers that are associated with some of the negative health consequences of obesity, namely fasting-state insulin levels (Pearson correlation: r=0.22, p=0.020, 95%-CI=[0.04, 0.39]), measures related to insulin—HOMA-IR, a marker of insulin resistance (Pearson correlation: r=0.24, p=0.015, 95%-CI=[0.05, 0.41], and C-peptide levels (Pearson correlation: r=0.23, p=0.018, 95%-CI=[0.04, 0.40])—and fasting-state leptin levels (Pearson correlation: r=0.34, p=0.001, 95%-CI=[0.16, 0.49]); see Figure 3c). All these associations remained significant when statistically controlling for age, education, total brain volume, and average head motion.

In Study 2, the correlation between predicted log(k) and BMI was positive but not significant (Pearson correlation: r=0.09, p=0.28, 95%-CI=[-0.07, 0.25]). However, paralleling the findings in Study 1, overweight-to-obese participants had a significantly higher k-marker response (higher predicted discounting) compared to lean participants (two-sample t-test: t(143)=2.11, p=0.037, Cohen's d=0.35, 95%-CI=[0.02, 0.57]; see Figure 3b).

Thresholded activation patterns of the k-marker

Activation patterns across the whole brain gray matter and across all three contrasts are used for prediction and cross-validation. To identify the areas that

contributed the most strongly with positive or negative weights, we used a bootstrapping procedure (5,000 samples). Bootstrapped weights were thresholded at q=0.05 FDR corrected across the whole weight map of the combined feature space (see Figure 2a and Figures 2-1, 2-2, and 2-3).

Our results revealed a distributed network of areas that jointly contributed to individual differences in delay discounting, including the vmPFC, ventral striatum, anterior midcingulate cortex (aMCC), hippocampus, frontoparietal, and visual areas (see Figure 2). Predictive activity patterns differed for the processes captured by the three different contrast images. Of note, some regions showed negative weights (i.e., predicted less discounting) for one contrast but positive weights (i.e., predicted more discounting) for another. For the Choice (versus implicit baseline) contrast, activity in the striatum, the anterior insula, and lateral prefrontal areas contributed positive weights for more discounting, whereas activity in visual, premotor, and motor areas contributed negative weights. For the parametric modulation by LL Amount, activity in vmPFC, aMCC, posterior cingulate cortex (PCC), precuneus, and frontoparietal areas contributed positive weights for greater discounting, whereas visual areas and premotor areas contributed mainly negative weights. For the parametric modulation by Delay, we observed positive weights in the most ventral part of the vmPFC, premotor areas, and visual cortex and negative weights in frontoparietal areas and brainstem regions.

To further assess the stability of weights, we tested whether developing the predictive model on the data of Study 2 and testing on Study 1 would yield comparable results. Training and cross-validating the model on the data of Study 2 resulted in similar prediction and transfer accuracy (Figure 4) and qualitatively similar weight maps (see Figure 4). At FDR-corrected level, voxels with significant weights in both directions (conjunction null, Nichols et al., 2005) for the LL Amount contrast were found in aMCC, bilateral anterior insula (AI), vmPFC, vlPFC, dlPFC, intraparietal sulcus (IPS), visual

cortex, and cerebellum. For the Delay contrast, significant weights in both directions were found in aMCC, dlPFC, parietal cortex, and AI. No voxels survived FDR correction in both directions for the Choice contrast.

Training predictive patterns on the three contrasts separately resulted in lower predictive accuracies (see Figure 5).

Similarity of k-marker brain patterns to meta-analytic maps

We next compared the predictive maps of the k-marker with term-based meta-analytic images (Yarkoni et al., 2011) for processes that may contribute to intertemporal decision-making. We computed the spatial correlation (Pearson's r) between the k-marker and meta-analytic maps for 1) affective- and value-related, 2) conflict- and cognitive control-related, and 3) memory-related terms (see Figure 6). While these spatial correlations are descriptive (c.f., Koban et al., 2019), they can inform us quantitatively whether and in which direction (positive or negative) previously identified functional networks contribute to individual differences in delay discounting.

Value- and affect-related maps (especially 'affect' and 'emotion') showed consistent positive correlations (r's > 0.05) with the Choice-related pattern of the k-marker, in line with the idea that more affect-related activity during intertemporal choices leads to more impatient decisions. However, stronger engagement of affective and especially 'reward'- and 'value'-related activity for increasing LL Amount (and, to a lesser extent, for increasing delays) was associated with less discounting. This suggests that lower discounting is associated with greater sensitivity of valuation-related signals to the amount of LL rewards.

In contrast to our initial hypothesis, more activity in cognitive control-related areas was not associated with lower discounting. Instead, there were positive correlations (r's from 0.05 to 0.19) of the Choice pattern with meta-analytic maps for 'attention', 'cognitive

control', 'conflict', and 'executive' (i.e., more positive weights predicting greater discounting). Further, stronger activation of control-related maps by greater LL Amount was associated with greater discounting, whereas stronger activation of control-related activity for longer delays was associated with less discounting.

Finally, we assessed the contribution of brain systems related to memory and prospection. While the term 'memory' (which also includes working-memory studies) showed a similar pattern as control-related maps, more specific terms such as 'episodic memory', 'imagery', and 'planning' were not substantially positively or negatively correlated with any of the k-marker patterns (r's around 0.05 and smaller).

Parallel findings were obtained when testing whether activity in non-overlapping meta-analytic maps (Yarkoni et al., 2011) (for value-related, cognitive control-related, or episodic memory-related activity) could separately predict log(k) (see Figure 7). Whereas areas associated with 'cognitive control' showed significant prediction in Study 1 and transfer to Study 2, areas associated with 'value' predicted discounting in Study 1 but no significant transfer to Study 2. Areas associated with 'episodic memory' showed only marginal prediction in Study 1 and no significant transfer to Study 2.

Local prediction of log(k)

Finally, we assessed whether activity patterns in smaller, more local brain areas could predict out-of-sample log(k) in Study 1 and whether such predictions would accurately transfer to Study 2. For this purpose, we used an established multi-modal cortical parcellation (Glasser et al., 2016) in combination with several other, subcortical parcellations, resulting in a total of 485 regions (publicly available at https://github.com/canlab/Neuroimaging_Pattern_Masks/tree/master/Atlases_and_parcellations/2018_Wager_combined_atlas). We trained and cross-validated a separate classifier for each region (combining functional activity across all three contrasts). For

each region we then tested whether the pattern trained on Study 1 data was predictive of individual differences in Study 2. Activity patterns that consistently predicted delay discounting in both studies were found in mid- and posterior cingulate cortex, right insula, and lateral frontal and parietal areas (see Figure 8 and Table 2), in line with the contributions of these areas in the whole-brain predictive pattern. In addition, activity patterns in amygdala, hippocampus, basal ganglia and brainstem areas (periaqueductal gray) also predicted individual differences in delay discounting in both studies.

Discussion

A major goal of neuroscience and psychiatry is to identify neuromarkers of transdiagnostic processes that are altered across different diseases or predispose individuals to such diseases (Insel and Cuthbert, 2015). Delay discounting—how much people prefer sooner compared to future rewards—has been proposed as such a transdiagnostic process across obesity and various forms of psychopathology, especially addiction and eating disorders (Bickel et al., 2014; Amlung et al., 2019; Lempert et al., 2019). In this paper, we advanced our understanding of the brain processes that drive variability in decision-making by identifying a distributed pattern of functional brain activity that predicts individual differences in delay discounting. We first used a cross-validation procedure to develop a novel functional brain marker of delay discounting (k-marker) based on whole-brain, gray matter-masked fMRI data (N_1=110). We then validated the k-marker (trained on Study 1 data only) in an independent second fMRI data set (N_2=145), sampled in a cohort with different socio-demographic characteristics, on a different fMRI scanner, and employing a different delay discounting task. Prediction-outcome correlations were 0.49 (Study 1) and 0.45 (Study 2), as large or larger than prediction of individual differences in other domains reported in previous studies (Rosenberg et al., 2016; Beaty et al., 2018; Han et al., 2021). In both studies, individual differences in

discounting were stable over time, and k-marker responses measured at baseline significantly predicted behavior several weeks later.

Recent findings have questioned the utility of brain imaging in predicting individual differences, especially for structural and resting-state fMRI data and for univariate, voxelwise-associations (Marek et al., 2022). An important advance of the present study is that it overcomes many of the limitations of previous studies by providing an independently cross-validated and multivariate 'brain model' (Kragel et al., 2018) of stable individual differences in impatient decision-making, in line with recent recommendations on studying brain-based prediction of individual differences (Rosenberg and Finn, 2022). As such, this brain model can be directly tested, validated, or refined in other existing or future fMRI data sets acquired during an intertemporal choice task. Its predictive performance can also be tested in clinical populations, such as patients with severe obesity, eating or substance use disorders, and other types of psychopathology.

Our results also inform the debate regarding the contributions of specific brain regions and functional networks to individual differences in delay discounting. Among the brain areas that contributed with positive and/or negative weights were the vmPFC, striatum, and other regions associated with valuation and reward (Levy and Glimcher, 2011; Bartra et al., 2013; Clithero and Rangel, 2014). This finding is in line with previous, univariate findings (Cooper et al., 2013; Pehlivanova et al., 2018; MacNiven et al., 2020). The present results add to this emergent picture by showing that greater sensitivity of reward- and value-related areas to the amount of the LL reward is linked to more patient decision-making.

Significant weights were found most consistently in the frontoparietal areas, midcingulate cortex, and anterior insula. Activity in these areas also allowed for significant prediction based on local activity alone (see Figure 8, ROI analysis). The dorsolateral prefrontal cortex has been theorized to implement self-control and far-sighted decision-

making (McClure et al., 2004; Hare et al., 2014). Yet the present results are surprising as they draw a more complex picture of these areas' contribution to delay discounting, with modulation of these areas by greater LL rewards being positively associated with discounting and modulation by delay being negatively associated with discounting. Thus, areas meta-analytically associated with cognitive control were more recruited for long delays and small LL amounts for low discounters, and for shorter delays and larger LL amounts for high discounters. These are the cases in which decisions are most difficult (closer to the indifference point) and therefore require resolution of response conflict (Botvinick et al., 2001; Kool et al., 2013; Shenhav et al., 2013; Hutcherson et al., 2020), or integration of expected value and risk of future rewards (Tobler et al., 2009).

These findings have implications for models of delay discounting and self-control in cognitive neuroscience. First, they speak against the idea of a simple dual process account of intertemporal choice and self-control (McClure et al., 2004), joining previous work that has suggested more complex neural processes at play (Kable and Glimcher, 2007; Ballard and Knutson, 2009; Hare et al., 2014; Berkman et al., 2017). Second, it also speaks against the idea that more frontoparietal activity is related to higher individual levels of self-control. Instead, it suggests that for which choice options control-related areas are activated is more informative than their overall level of activation. This finding is in line with value-based choice models of self-control (Berkman et al., 2017) and with recent evidence that high and low discounters differ in how much attention they allocate to amount versus delay information (Amasino et al., 2019). It also fits with the idea that low discounters may not need 'control' to discount less (Lempert et al., 2019), and that high discounters may employ cognitive control for different types of decisions.

In line with the importance of prospection and self-projection in intertemporal decision-making, the hippocampus and adjacent midtemporal areas have been associated with individual differences in discounting (Benoit et al., 2011; Peters and

Büchel, 2011; Lebreton et al., 2013). The k-marker has significant weights in parahippocampal areas and in occipital areas, but the weight maps were not strongly associated with broader meta-analysis-based activation maps of episodic memory or prospection, possibly because those masks also include many areas that are involved in processes other than memory and prospection. In agreement with the k-marker results and the literature described above, our ROI-based results showed significant local prediction of individual differences in delay discounting in hippocampus, amygdala and the memory-related anteromedial thalamus.

Our findings highlight the importance of investigating distributed brain activity patterns, confirming the notion that delay discounting depends on the interactions among different functional processes and networks in the brain. In addition to frontoparietal areas, midcingulate, and hippocampus, several other cortical and subcortical areas also allowed for cross-validated local prediction of individual differences in delay discounting, across both data sets. Consistent with the whole-brain results, these included several areas in the mid and posterior insula, which is involved in interoception (Craig, 2009), salience (Bartra et al., 2013), and exploration (Zhen et al., 2022)—processes which may all be involved in delay discounting. Local prediction was also found in subcortical areas associated with affect and visceromotor control, including the amygdala and the periaqueductal gray.

Previous work has related individual differences in delay discounting with obesity, substance use disorders, and psychiatric diseases (Peters and Büchel, 2011; Amlung et al., 2019; Lempert et al., 2019). In the two samples presented here, log(k) values based on participants' choices themselves were not significantly associated with BMI or overweight. However, the two studies were not designed to include a large range of BMI or many obese participants, and obesity-related alterations in discounting might be more pronounced for food than monetary rewards. While in Study 1 participants' height and

weight were measured by the experimenters, these values were self-reported in Study 2, which might explain the lower associations with BMI in Study 2.

In contrast to discounting behavior, responses to the k-marker did significantly differ between lean and overweight participants and predicted out-of-sample blood markers related to glucose and fat metabolism. These findings suggest that this functional brain marker reflects variance in neurophysiology that is related to stable long-term patterns in decision-making and health. The k-marker even seemed more sensitive to individual differences than the behavioral measures it was trained on, potentially because it is a closer reflection of the neurophysiological underpinnings that drive both discounting behavior and more distal health outcomes, in line with previous evidence that brain-based can outperform behavior-based prediction (Genevsky et al., 2017). Of note, our approach is cross-sectional and remains agnostic regarding potential causal links among brain function, behavior, and body weight. While higher discounting is typically considered a causal or predisposing factor for weight gain, an alternative hypothesis is that overweight and changes in metabolism lead to changes in brain physiology and subsequent behavioral outcomes (Cornil et al., 2021; Schmidt et al., 2021). Future work can test the k-marker in larger numbers of participants with obesity and other health conditions.

In conclusion, the k-marker—a novel fMRI-based brain signature—predicts individual differences in intertemporal decision-making in neurotypical, healthy adults across different populations, scanners, and analysis pipelines. It can be quantitatively tested in any other fMRI study on delay discounting for which contrast images for Choice, LL Amount, and Delay can be computed, including in other delay discounting paradigms, such as those that involve non-monetary rewards such as food or social discounting tasks (Jones and Rachlin, 2006; Strombach et al., 2015). Future work could test the generalizability of the k-marker in children, adolescents, the elderly, or clinical populations. Most importantly, future work will show whether the k-marker prospectively predicts clinical

status and health outcomes in conditions related to abnormal discounting, such as eating disorders, substance use, and other psychiatric disorders.

Data and code availability statement

Data from Study 2 is available in an online public repository (doi: 10.18112/openneuro.ds002843.v1.0.0). Deidentified data from Study 1 will be made available upon publication. The resulting classifier patterns (k-marker) and code to apply it to other datasets is available at: https://github.com/ldmk/k-marker. Code for analyses is available at https://github.com/canlab and upon request to the first author.

References

Amasino DR, Sullivan NJ, Kranton RE, Huettel SA (2019) Amount and time exert independent influences on intertemporal choice. Nat Hum Behav 3:383-392.

Amlung M, Petker T, Jackson J, Balodis I, MacKillop J (2016) Steep discounting of delayed monetary and food rewards in obesity: a meta-analysis. Psychol Med 46:2423-2434.

Amlung M, Marsden E, Holshausen K, Morris V, Patel H, Vedelago L, Naish KR, Reed DD, McCabe RE (2019) Delay Discounting as a Transdiagnostic Process in Psychiatric Disorders: A Meta-analysis. JAMA Psychiatry 76:1176-1186.

Anokhin AP, Golosheykin S, Mulligan RC (2015) Long-term test-retest reliability of delayed reward discounting in adolescents. Behav Processes 111:55-59.

Audrain-McGovern J, Rodriguez D, Epstein LH, Cuevas J, Rodgers K, Wileyto EP (2009) Does delay discounting play an etiological role in smoking or is it a consequence of smoking? Drug Alcohol Depend 103:99-106.

Ballard K, Knutson B (2009) Dissociable neural representations of future reward magnitude and delay during temporal discounting. Neuroimage 45:143-150.

Bär K-J, de la Cruz F, Schumann A, Koehler S, Sauer H, Critchley H, Wagner G (2016) Functional connectivity and network analysis of midbrain and brainstem nuclei. Neuroimage 134:53-63.

Bartra O, McGuire JT, Kable JW (2013) The valuation system: a coordinate-based meta-analysis of BOLD fMRI experiments examining neural correlates of subjective value. Neuroimage 76:412-427.

Beaty RE, Kenett YN, Christensen AP, Rosenberg MD, Benedek M, Chen Q, Fink A, Qiu J, Kwapil TR, Kane MJ, Silvia PJ (2018) Robust prediction of individual creative ability from brain functional connectivity. Proc Natl Acad Sci U S A 115:1087-1092.

Benoit RG, Gilbert SJ, Burgess PW (2011) A neural mechanism mediating the impact of episodic prospection on farsighted decisions. J Neurosci 31:6771-6779.

Berkman ET, Hutcherson CA, Livingston JL, Kahn LE, Inzlicht M (2017) Self-Control as Value-Based Choice. Curr Dir Psychol Sci 26:422-428.

Berman MG, Yourganov G, Askren MK, Ayduk O, Casey BJ, Gotlib IH, Kross E, McIntosh AR, Strother S, Wilson NL, Zayas V, Mischel W, Shoda Y, Jonides J (2013) Dimensionality of brain networks linked to life-long individual differences in self-control. Nat Commun 4:1373.

Bickel WK, Odum AL, Madden GJ (1999) Impulsivity and cigarette smoking: delay discounting in current, never, and ex-smokers. Psychopharmacology 146:447-454.

Bickel WK, George Wilson A, Franck CT, Terry Mueller E, Jarmolowicz DP, Koffarnus MN, Fede SJ (2014) Using crowdsourcing to compare temporal, social temporal, and probability discounting among obese and non-obese individuals. Appetite 75:82-89.

Botvinick MM, Braver TS, Barch DM, Carter CS, Cohen JD (2001) Conflict monitoring and cognitive control. Psychol Rev 108:624-652.

Clithero JA, Rangel A (2014) Informatic parcellation of the network involved in the computation of subjective value. Soc Cogn Affect Neurosci 9:1289-1302.

Cooper N, Kable JW, Kim BK, Zauberman G (2013) Brain activity in valuation regions while thinking about the future predicts individual discount rates. J Neurosci 33:13150-13156.

Cornil Y, Plassmann H, Aron-Wisnewsky J, Poitou-Bernert C, Clément K, Chabert M, Chandon P (2021) Obesity and responsiveness to food marketing before and after bariatric surgery. J Consum Psychol.

Craig ADB (2009) How do you feel--now? The anterior insula and human awareness. Nat Rev Neurosci 10:59-70.

Diedrichsen J, Balsters JH, Flavell J, Cussans E, Ramnani N (2009) A probabilistic MR atlas of the human cerebellum. Neuroimage 46:39-46.

Fernie G, Peeters M, Gullo MJ, Christiansen P, Cole JC, Sumnall H, Field M (2013) Multiple behavioural impulsivity tasks predict prospective alcohol involvement in adolescents. Addiction 108:1916-1923.

Gabrieli JDE, Ghosh SS, Whitfield-Gabrieli S (2015) Prediction as a humanitarian and pragmatic contribution from human cognitive neuroscience. Neuron 85:11-26.

Genevsky, A., Yoon, C., and Knutson, B. (2017). When brain beats behavior: neuroforecasting crowdfunding outcomes. J Neurosci 37:8625–8634.

Glasser MF, Coalson TS, Robinson EC, Hacker CD, Harwell J, Yacoub E, Ugurbil K, Andersson J, Beckmann CF, Jenkinson M, Smith SM, Van Essen DC (2016) A multi-modal parcellation of human cerebral cortex. Nature 536:171-178.

Han X, Ashar YK, Kragel P, Petre B, Schelkun V, Atlas LY, Chang LJ, Jepma M, Koban L, Losin EAR, Roy M, Woo C-W, Wager TD (2021) Effect sizes and test-retest reliability of the fMRI-based Neurologic Pain Signature. Neuroimage:118844.

Hare TA, Hakimi S, Rangel A (2014) Activity in dlPFC and its effective connectivity to vmPFC are associated with temporal discounting. Front Neurosci 8:50.

Hutcherson CA, Rangel A, Tusche A (2020) Evidence accumulation, not" self-control," explains why the dlPFC activates during normative choice. bioRxiv.

Insel TR, Cuthbert BN (2015) Medicine. Brain disorders? Precisely. Science 348:499-500.

Jarmolowicz DP, Cherry JBC, Reed DD, Bruce JM, Crespi JM, Lusk JL, Bruce AS (2014) Robust relation between temporal discounting rates and body mass. Appetite 78:63-67.

Jones B, Rachlin H (2006) Social discounting. Psychol Sci 17:283-286.

Kable JW, Glimcher PW (2007) The neural correlates of subjective value during intertemporal choice. Nat Neurosci 10:1625-1633.

Kable JW, Caulfield MK, Falcone M, McConnell M, Bernardo L, Parthasarathi T, Cooper N, Ashare R, Audrain-McGovern J, Hornik R, Diefenbach P, Lee FJ, Lerman C (2017) No Effect of Commercial Cognitive Training on Brain Activity, Choice Behavior, or Cognitive Performance. J Neurosci 37:7390-7402.

Kirby KN (2009) One-year temporal stability of delay-discount rates. Psychon Bull Rev 16:457-462.

Kirby KN, Herrnstein RJ (1995) Preference Reversals Due to Myopic Discounting of Delayed Reward. Psychol Sci 6:83-89.

Koban L, Jepma M, López-Solà M, Wager TD (2019) Different brain networks mediate the effects of social and conditioned expectations on pain. Nat Commun 10:4096.

Kool W, McGuire JT, Wang GJ, Botvinick MM (2013) Neural and behavioral evidence for an intrinsic cost of self-control. PLoS One 8:e72626.

Kragel PA, Koban L, Barrett LF, Wager TD (2018) Representation, Pattern Information, and Brain Signatures: From Neurons to Neuroimaging. Neuron 99:257-273.

Lebreton M, Bertoux M, Boutet C, Lehericy S, Dubois B, Fossati P, Pessiglione M (2013) A critical role for the hippocampus in the valuation of imagined outcomes. PLoS Biol 11:e1001684.

Lempert KM, Phelps EA (2016) The Malleability of Intertemporal Choice. Trends Cogn Sci 20:64-74.

Lempert KM, Steinglass JE, Pinto A, Kable JW, Simpson HB (2019) Can delay discounting deliver on the promise of RDoC? Psychol Med 49:190-199.

Levy DJ, Glimcher PW (2011) Comparing apples and oranges: using reward-specific and reward-general subjective value representation in the brain. J Neurosci 31:14693-14707.

Li N, Ma N, Liu Y, He X-S, Sun D-L, Fu X-M, Zhang X, Han S, Zhang D-R (2013) Resting-state functional connectivity predicts impulsivity in economic decision-making. J Neurosci 33:4886-4895.

Lozano R et al. (2012) Global and regional mortality from 235 causes of death for 20 age groups in 1990 and 2010: a systematic analysis for the Global Burden of Disease Study 2010. Lancet 380:2095-2128.

MacKillop J, Amlung MT, Few LR, Ray LA, Sweet LH, Munafò MR (2011) Delayed reward discounting and addictive behavior: a meta-analysis. Psychopharmacology 216:305-321.

MacNiven KH, Leong JK, Knutson B (2020) Medial forebrain bundle structure is linked to human impulsivity. Sci Adv 6:eaba4788.

Marek S et al. (2022) Reproducible brain-wide association studies require thousands of individuals. Nature 603:654-660.

McClure SM, Laibson DI, Loewenstein G, Cohen JD (2004) Separate neural systems value immediate and delayed monetary rewards. Science 306:503-507.

Mole TB, Irvine MA, Worbe Y, Collins P, Mitchell SP, Bolton S, Harrison NA, Robbins TW, Voon V (2015) Impulsivity in disorders of food and drug misuse. Psychol Med 45:771-782.

Nichols T, Brett M, Andersson J, Wager T, Poline J-B (2005) Valid conjunction inference with the minimum statistic. Neuroimage 25:653-660.

Pauli WM, O'Reilly RC, Yarkoni T, Wager TD (2016) Regional specialization within the human striatum for diverse psychological functions. Proc Natl Acad Sci U S A 113:1907-1912.

Pehlivanova M, Wolf DH, Sotiras A, Kaczkurkin AN, Moore TM, Ciric R, Cook PA, Garcia de La Garza A, Rosen AFG, Ruparel K, Sharma A, Shinohara RT, Roalf DR, Gur RC, Davatzikos C, Gur RE, Kable JW, Satterthwaite TD (2018) Diminished Cortical

Thickness Is Associated with Impulsive Choice in Adolescence. J Neurosci 38:2471-2481.

Peters J, Büchel C (2011) The neural mechanisms of inter-temporal decision-making: understanding variability. Trends Cogn Sci 15:227-239.

Poldrack RA, Huckins G, Varoquaux G (2020) Establishment of Best Practices for Evidence for Prediction: A Review. JAMA Psychiatry 77:534-540.

Poldrack RA, Baker CI, Durnez J, Gorgolewski KJ, Matthews PM, Munafò MR, Nichols TE, Poline J-B, Vul E, Yarkoni T (2017) Scanning the horizon: towards transparent and reproducible neuroimaging research. Nat Rev Neurosci 18:115-126.

Rosenberg MD, Finn ES (2022) How to establish robust brain–behavior relationships without thousands of individuals. Nat Neurosci:1-3.

Rosenberg MD, Casey BJ, Holmes AJ (2018) Prediction complements explanation in understanding the developing brain. Nat Commun 9:589.

Rosenberg MD, Finn ES, Scheinost D, Papademetris X, Shen X, Constable RT, Chun MM (2016) A neuromarker of sustained attention from whole-brain functional connectivity. Nat Neurosci 19:165-171.

Rosenberg MD, Martinez SA, Rapuano KM, Conley MI, Cohen AO, Cornejo MD, Hagler DJ, Jr., Meredith WJ, Anderson KM, Wager TD, Feczko E, Earl E, Fair DA, Barch DM, Watts R, Casey BJ (2020) Behavioral and neural signatures of working memory in childhood. J Neurosci 40:5090-5104.

Scheinost D, Noble S, Horien C, Greene AS, Lake EM, Salehi M, Gao S, Shen X, O'Connor D, Barron DS, Yip SW, Rosenberg MD, Constable RT (2019) Ten simple rules for predictive modeling of individual differences in neuroimaging. Neuroimage 193:35-45.

Schmidt L, Medawar E, Aron-Wisnewsky J, Genser L, Poitou C, Clément K, Plassmann H (2021) Resting-state connectivity within the brain's reward system predicts weight loss and correlates with leptin. Brain communications 3:fcab005.

Shen X, Tokoglu F, Papademetris X, Constable RT (2013) Groupwise whole-brain parcellation from resting-state fMRI data for network node identification. Neuroimage 82:403-415.

Shenhav A, Botvinick MM, Cohen JD (2013) The expected value of control: an integrative theory of anterior cingulate cortex function. Neuron 79:217-240.

Strombach T, Weber B, Hangebrauk Z, Kenning P, Karipidis II, Tobler PN, Kalenscher T (2015) Social discounting involves modulation of neural value signals by temporoparietal junction. Proc Natl Acad Sci U S A 112:1619-1624.

Tibshirani R (1996) Regression Shrinkage and Selection Via the Lasso. J R Stat Soc Series B Stat Methodol 58:267-288.

Tobler PN, Christopoulos GI, O'Doherty JP, Dolan RJ, Schultz W (2009) Risk-dependent reward value signal in human prefrontal cortex. Proc Natl Acad Sci U S A 106:7185-7190.

van den Bos W, Rodriguez CA, Schweitzer JB, McClure SM (2014) Connectivity strength of dissociable striatal tracts predict individual differences in temporal discounting. J Neurosci 34:10298-10310.

Wager TD, Atlas LY, Leotti LA, Rilling JK (2011) Predicting individual differences in placebo analgesia: contributions of brain activity during anticipation and pain experience. J Neurosci 31:439-452.

Wager TD, Atlas LY, Lindquist MA, Roy M, Woo C-W, Kross E (2013) An fMRI-based neurologic signature of physical pain. N Engl J Med 368:1388-1397.

Woo C-W, Chang LJ, Lindquist MA, Wager TD (2017) Building better biomarkers: brain models in translational neuroimaging. Nat Neurosci 20:365-377.

Yarkoni T, Poldrack RA, Nichols TE, Van Essen DC, Wager TD (2011) Large-scale automated synthesis of human functional neuroimaging data. Nat Methods 8:665-670.

Yu H, Koban L, Chang LJ, Wagner U, Krishnan A, Vuilleumier P, Zhou X, Wager TD (2020) A Generalizable Multivariate Brain Pattern for Interpersonal Guilt. Cereb Cortex 30:3558-3572.

Zhen S, Yaple ZA, Eickhoff SB, Yu R (2022) To learn or to gain: neural signatures of exploration in human decision-making. Brain Struct Funct 227:63-76.

Tables

Table 1. Person-level characteristics of lean (BMI <= 25) and overweight-to-obese (BMI > 25) participants in Study 1 and Study 2. Except for body mass (by definition) and k-marker responses, none of the variables differed significantly between the two groups.

Study 1	BMI <= 25	BMI > 25	two-sample t-test		
	M(STD)	M(STD)	t(df)	p-value	CI
N	52	58			
BMI	23.0 (1.3)	27.8 (2.2)	-13.8 (108)	<0.001*	[-5.51, -4.13]
Log(k)	-5.71 (1.83)	-5.70 (2.04)	-0.04 (108)	0.96	[-0.75, 0.72]
k-marker	-5.87 (0.76)	-5.46 (0.74)	-2.85 (108)	0.005*	[-0.69, -0.12]
Age (y)	30.8 (10.4)	32.4 (9.8)	-0.85 (108)	0.40	[-5.43, 2.17]
Education (ordinal scale)	5.09 (2.71)	5.05 (2.89)	0.08 (108)	0.93	[-1.02, 1.11]
Total brain volume (l)	1.17 (0.09)	1.18 (0.09)	-0.62 (108)	0.53	[-0.04, 0.02]

Study 2	BMI <= 25	BMI > 25	two-sample t-test		
	M(STD)	M(STD)	t(df)	p-value	CI
N	81	64			
BMI	22.2 (1.8)	29.4 (3.9)	-14.9 (143)	<0.001*	[-8.18, -6.27]
Log(k)	-4.09 (1.00)	-4.08 (0.83)	-0.08 (143)	0.94	[-0.32, 0.30]
k-marker	-5.86 (0.90)	-5.57 (0.74)	-2.1 (143)	0.037*	[-0.57, -0.02]
Age	24.2 (4.5)	24.6 (4.5)	-0.57 (143)	0.57	[-1.93, 1.07]
Education	3.31 (0.93)	3.39 (0.81)	-0.56 (143)	0.58	[-0.37, 0.21]
Total brain volume (l)	1.26 (0.12)	1.26 (0.12)	-0.11 (143)	0.91	[-0.04, 0.04]
				chi^2-test	

Sex			chi^2	p-value
–Male (N)	46	42	1.17 (1)	0.28
–Female (N)	35	22		

Table 2. ROI-based prediction of individual differences in log(k). This analysis used an existing atlas of the brain, including 485 regions based on several different previous parcellations (Diedrichsen et al., 2009; Shen et al., 2013; Bär et al., 2016; Glasser et al., 2016; Pauli et al., 2016) available at: https://github.com/canlab/Neuroimaging_Pattern_Masks/tree/master/Atlases_and_parcellations/2018_Wager_combined_atlas). Predictive patterns were trained and cross-validated on Study 1 data only (using the same procedures as for the global classifier) and then tested in Study 2. The table below shows only brain parcels that had significant prediction in both data sets (p-values are uncorrected for multiple comparisons). Note that each parcel contains many voxels, each of which may contribute with positive and/or negative weights to delay discounting for each of the three contrast images.

			Study 1 (training and cross-validation)		Study 2 (test)	
Area name	Area description	Hemisphere	Prediction-outcome *r*	p-value	Prediction-outcome *r*	p-value
RSC	RetroSplenial Complex	L	0.30	0.010	0.21	0.010
RSC	RetroSplenial Complex	R	0.23	0.049	0.21	0.013
23d	Area dorsal 23	L	0.23	0.042	0.17	0.043
7Am	Medial Area 7a	L	0.23	0.045	0.22	0.007
7Am	Medial Area 7a	R	0.30	0.009	0.28	0.001
7PC	Area 7PC	R	0.28	0.016	0.20	0.014
Area1	Area 1	L	0.23	0.037	0.18	0.035
p24pr	Area posterior 24 prime	L	0.30	0.014	0.21	0.011

a24pr	Area anterior 24 prime	L	0.38	0.001	0.21	0.013
a24pr	Area anterior 24 prime	R	0.37	0.001	0.21	0.010
p32pr	Area posterior 32 prime	L	0.43	0.000	0.20	0.016
d32	Area dorsal 32	L	0.36	0.002	0.24	0.004
d32	Area dorsal 32	R	0.28	0.016	0.34	0.000
8BM	Area 8BM	L	0.25	0.033	0.29	0.000
8BM	Area 8BM	R	0.30	0.012	0.26	0.001
13l	Area 13I	R	0.25	0.025	-0.16	0.048
6a	Area 6 anterior	R	0.40	0.001	0.30	0.000
PoI2	Posterior Insular Area 2	R	0.35	0.004	0.21	0.009
MI	Middle Insular Area	R	0.23	0.040	0.39	0.000
AVI	Anterior Ventral Insular Area	R	0.30	0.009	0.43	0.000
TPOJ3	Temporoparietooccipital Junction 3	R	0.28	0.017	0.20	0.018
IP1	Area lntraParietal11	R	0.29	0.013	0.23	0.006
PFm	Area PFm Complex	R	0.25	0.028	0.24	0.003
PoI1	Posterior Insular Area 1	R	0.24	0.041	0.27	0.001
FOP5	Area Frontal Opercular 5	R	0.27	0.022	0.36	0.000
GPi	Internal globus pallidus	R	0.23	0.046	0.23	0.005
Thal_AM	Anteromedial thalamic nucleus	L	0.27	0.024	0.19	0.020

Bstem Midbd	Brainstem midbrain	L	0.23	0.047	0.22	0.008
Bstem PAG	Brainstem periaqueductal gray	R&L	0.39	0.001	0.19	0.023
Hippocampus CA2	Hippocampus area CA2	R&L	0.22	0.040	0.20	0.015
Amygdala CM	Centromedial amygdala	R&L	0.22	0.038	0.17	0.042

Figure Legends

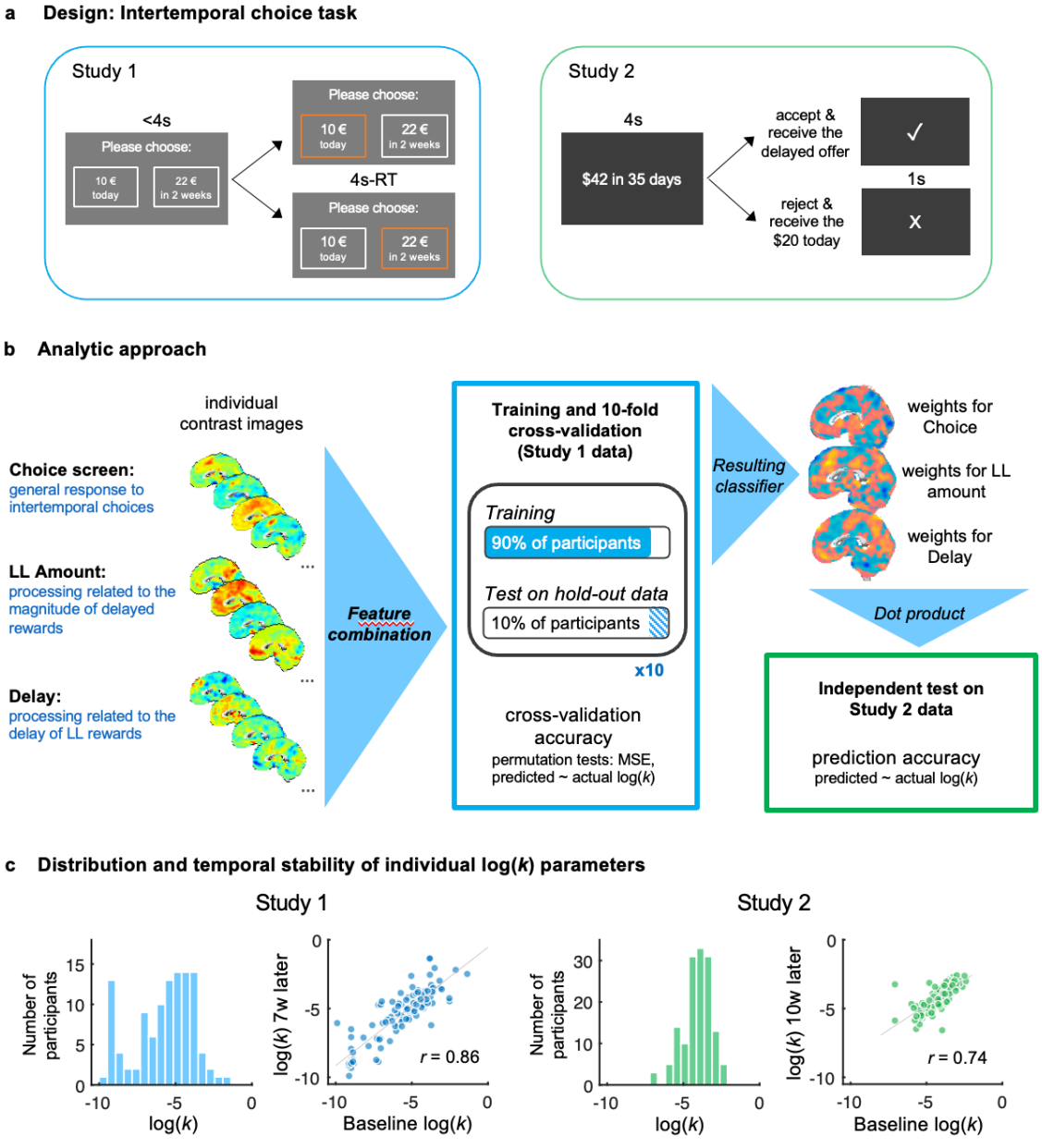

Figure 1. Experimental design, analytical approach, and discounting behavior. a) Visual presentation of the intertemporal choice tasks and their timing in Study 1 and Study 2. All combinations of amounts and delays can be found in Extended Data tables Figure 1-1 (for Study 1) and Figure 1-2 (for Study 2). **b)** Analytic approach. Contrast

images for brain activity in response to the onset of the Choice screen and its parametric modulation by LL Amount and Delay were computed for each participant and concatenated. Data from Study 1 was used for training and 10-fold cross-validation. In each fold, the classifier was trained on 90% of the data using LASSO-PCR and tested on the remaining 10% hold-out data to evaluate its predictive accuracy. The predictive classifier obtained from Study 1 was then tested on Study 2 data, acquired on a different scanner, in a different lab and country, assessing its validity in a completely independent data set. **c)** Distribution and temporal stability of individual log-transformed k-parameters by study. Scatterplots show high correlations between individual differences in discounting at baseline and several weeks later (Study 1: N=110, r=0.86, p=0.001, 95% CI=[0.80, 0.90], Study 2: N=145, r=0.74, p=0.001, 95%-CI=[0.63, 0.82]).

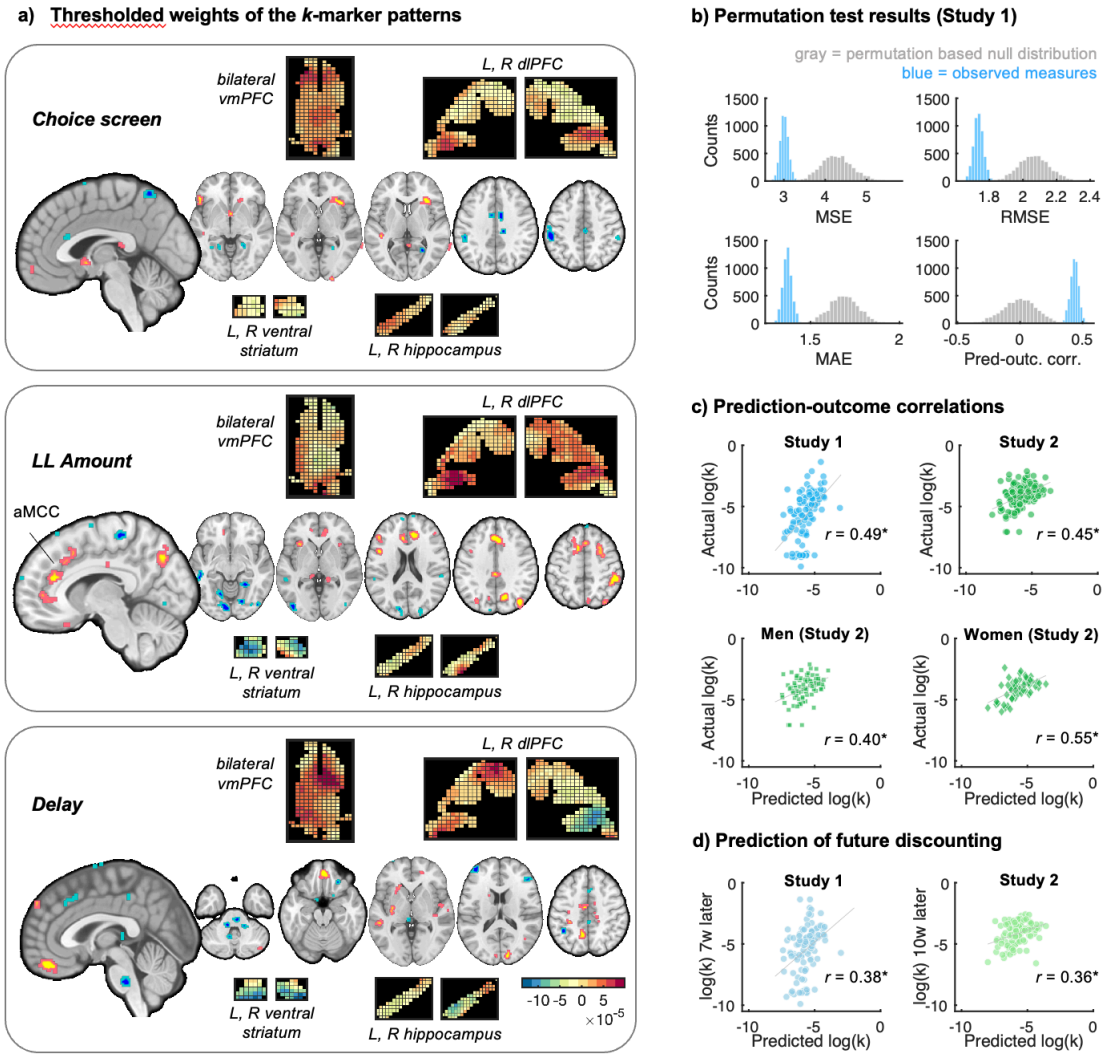

Figure 2. Weight maps and predictive accuracy of the classifier ('k-marker'). a) Classifier weights for the three contrast images (Choice screen onset, parametric modulation by LL Amount and Delay), thresholded for illustration at q=0.05 FDR corrected across the combined feature space (three concatenated maps). See Extended Data Figure 2-1, Figure 2-2, and Figure 2-3 for coordinate tables. Note that unthresholded maps are used for prediction and that the combined weights across maps are contributing to the prediction. Pop-out maps show the unthresholded patterns for selected regions of interest (transversal slices for vmPFC, coronal for dlPFC, and saggital for hippocampus), in order to illustrate the heterogeneity of voxel weights (e.g., positive versus negative) within each

region and across the three interdependent weight maps. **b)** Results of the permutation tests (Study 1). Log(k) values were randomly permuted, and the prediction algorithm was repeated on the permuted brain-outcome data 5000 times to generate null distributions (in gray) for standard accuracy metrics (from left to right): mean squared error (MSE), root mean squared error (RMSE), mean absolute error (mean abs error), and prediction-outcome correlation (all *p*-values < 0.0002). In addition, observed metrics in 5000 random cross-validation folds are shown in blue bars. **c)** For interpretability and comparability across both studies, prediction–outcome correlations are shown as scatterplots, for Study 1 (N=110, r=0.49, p<0.001, permutation test) and Study 2 (independent validation data set, parametric prediction–outcome correlation, N=145, r=0.45, p<0.001, 95%-CI=[0.31, 0.57]). Correlations between predicted and observed log(k) were significant in both male and female participants (Study 2). **d)** Prediction of future discounting. Responses of the k-marker responses at baseline significantly predict individual differences in log(k) seven weeks later in Study 1 (left panel, N=109, r=0.38, p=0.001, 95%-CI=[0.20, 0.53]) and ten weeks later in Study 2 (right panel, N=102, r=0.36, p=0.002, 95%-CI=[0.17, 0.51]).

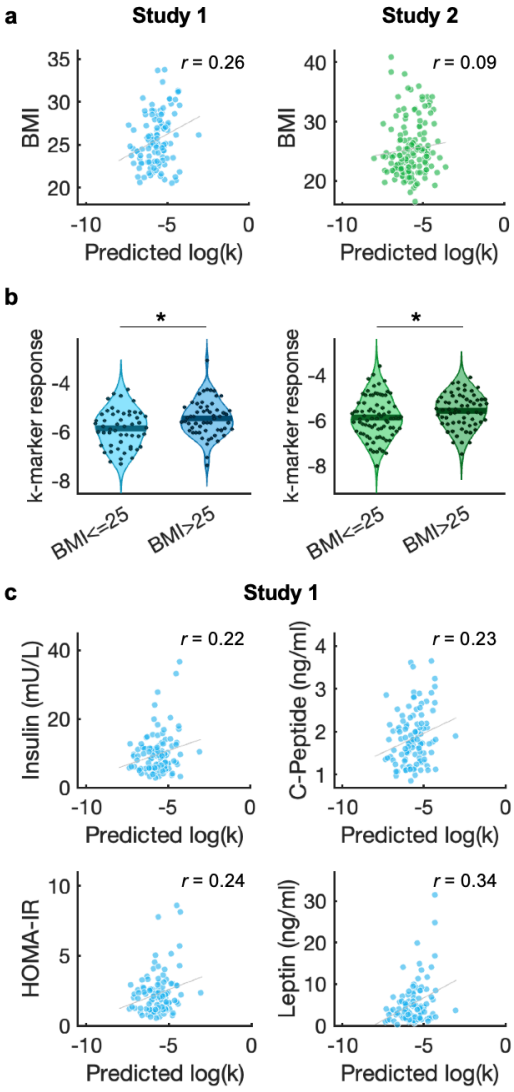

Figure 3. Association of k-marker response with BMI, overweight, and metabolic blood markers. a) The k-marker response was positively and significantly correlated with BMI in Study 1 (N=110, r=0.26, p=0.005, 95%-CI=[0.08, 0.43]), but not significantly in Study 2 (N=145, r=0.09, p=0.28, 95%-CI=[-0.07, 0.25]). **b)** In both studies, k-marker response was significantly greater (predicting more delay discounting) in overweight (BMI > 25) compared to lean participants (Study 1: t(108)=2.85, p=0.005, Cohen's d=0.55, 95%-CI=[0.12, 0.69]; Study 2: t(143)=2.11, p=0.037, Cohen's d=0.35, 95%-CI=[0.02, 0.57]). Lean and overweight participants did not differ on any demographic variables in both studies (see Table 1). **c)** Individual differences in out-of-sample k-marker response

in Study 1 were positively and significantly correlated with serum insulin (N=110, r=0.22, p=0.020, 95%-CI=[0.04, 0.39]), C-peptide (N=110, r=0.23, p=0.018, 95%-CI=[0.04, 0.40]), insulin resistance (as measured by the HOMA-IR index, N=105, r=0.24, p=0.015, 95%-CI=[0.05, 0.41]), and leptin (N=102, r=0.34, p=0.001, 95%-CI=[0.16, 0.49]).

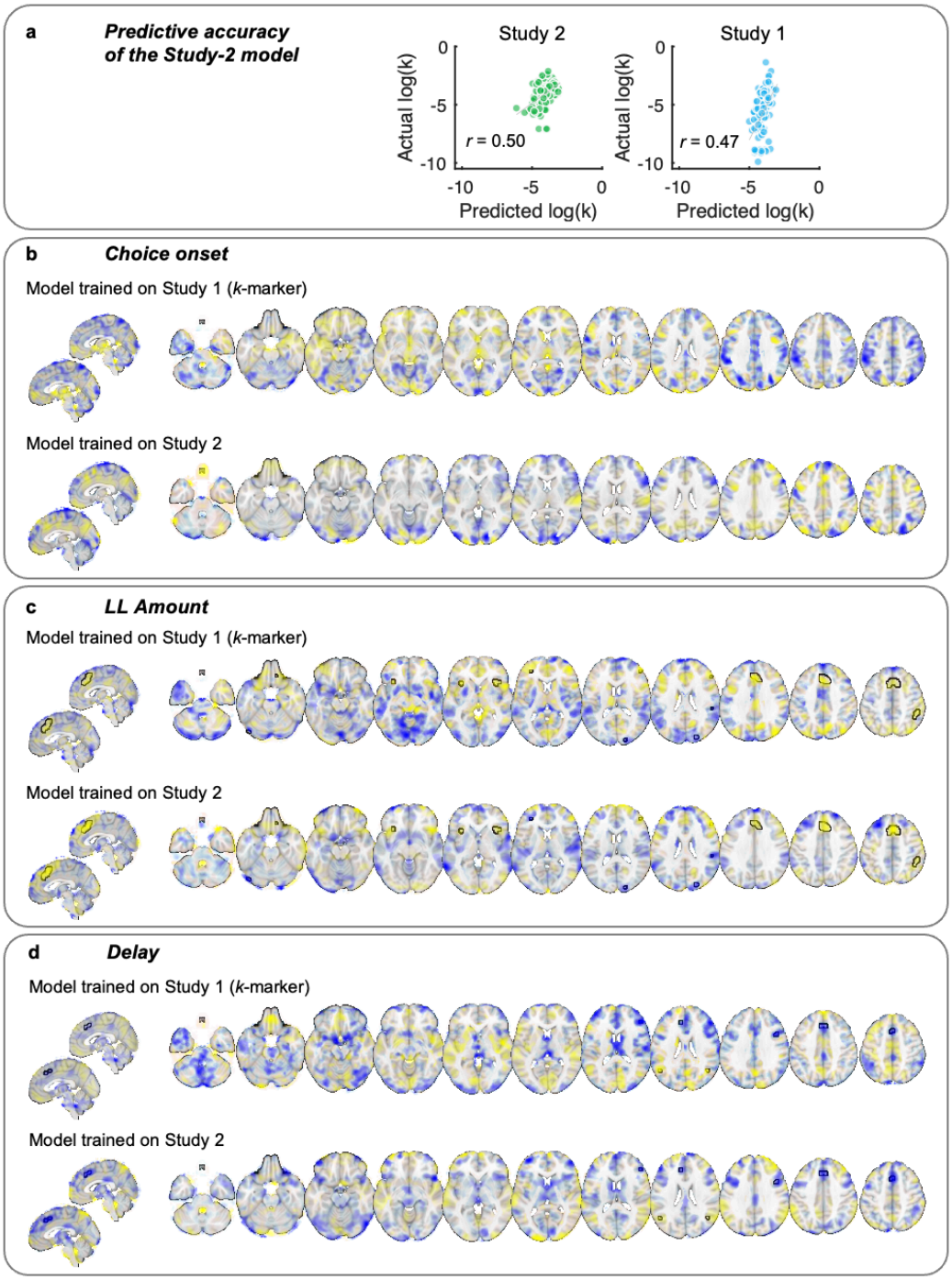

Figure 4. Results for an alternative model trained on the data of Study 2 and comparison of weight maps (control analysis). a) Training and cross-validating an alternative predictive model on the data of Study 2 (N=145) resulted in a prediction-outcome correlation of r=0.50 (comparable to the original predictive model) and a

prediction R^2=0.25. Testing this model on the data of Study 1 (N=110, as an independent test set) resulted in a prediction-outcome correlation of r=0.47 and a prediction R^2=-0.61. The contrast-wise unthresholded weight maps of the two different predictive models are displayed in panels **b)** (for the Choice contrast), **c)** (LL-Amount), and **d)** (Delay). Yellow indicates positive and blue indicates negative voxel weights, with lower transparencies indicating stronger absolute weights. Black outlines reflect the conjunction of significant feature weights in both models (at P < 0.05 corrected for multiple comparisons in each model). The correlation between feature weights correlated of the two models was r=0.09 (across all three maps). Correlations for the LL-Amount (r=0.10) and Delay contrast (r=0.11) were numerically higher than for the Choice screen contrast (r=0.05).

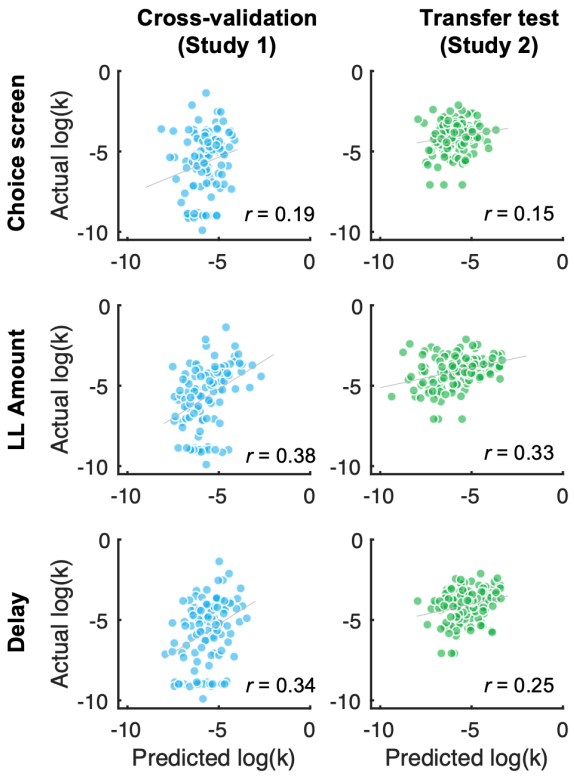

Figure 5. Results (prediction-outcome correlations) for training separate predictive models for each of the three contrasts (control analysis). To assess their distinct

contributions, we trained three separate predictive models on each of the three contrast maps of Study 1 and tested them on the corresponding contrast maps of Study 2 (using the same algorithm and cross-validation procedure as before). The results showed modest predictive accuracy for the model trained on the Choice screen contrast only (top row), with a prediction-outcome correlation of $r = 0.19$ in Study 1 (training and cross-validation set, $p = 0.10$ based on permutation test, 5000 iterations) and of $r = 0.15$ in Study 2 ($p = 0.07$). Training a model based on the LL-Amount contrast had a significant prediction-outcome correlation of $r = 0.38$ in Study 1 ($p < 0.001$, permutation test) and of $r = 0.34$ ($p < 0.001$) in Study 2. Similarly, training a model on the Delay contrast resulted in a significant prediction-outcome correlation of $r = 0.34$ in Study 1 ($p = 0.014$, permutation test) and of $r = 0.25$ ($p = 0.002$) in Study 2. Thus, none of the separate models achieved similarly high predictive performance as the combined model (three concatenated contrasts), especially regarding transfer to Study 2.

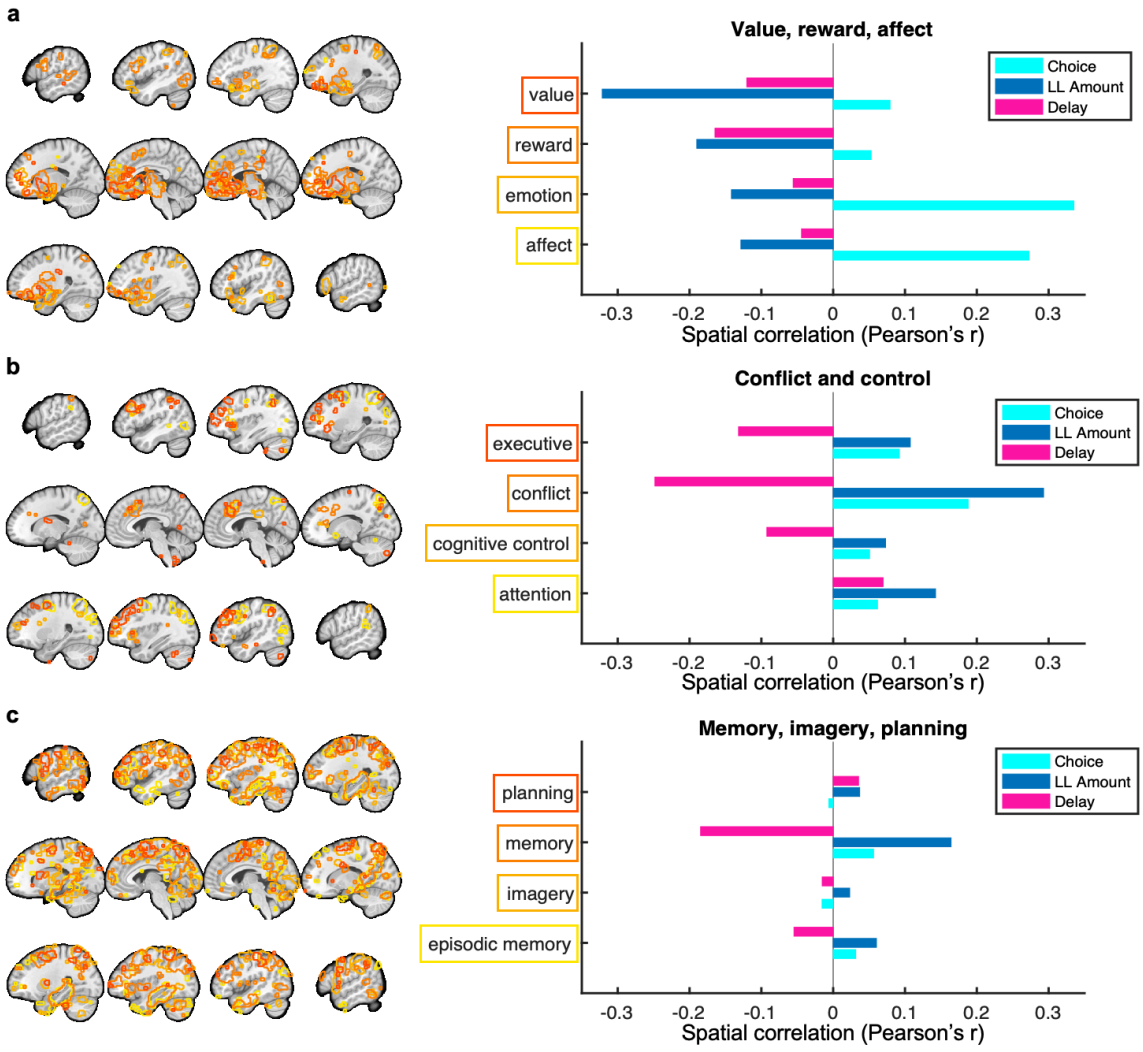

Figure 6. Spatial similarity of the k-marker with meta-analytic maps. In order to quantitatively compare the classifier patterns with theoretically relevant functional networks, we computed the spatial correlation of the unthresholded k-marker patterns with thresholded Neurosynth meta-analytic maps (Yarkoni et al., 2011) associated with **a**) value, reward and affect, **b**) conflict and control, and **c**) memory, imagery, and planning. Meta-analytic maps from each group of terms are overlaid on the left (outline colors matching the outlines of the terms on the right) and can be inspected in greater detail online (www.Neurosynth.org). Note that spatial correlations are purely descriptive, indicating whether activity in any of the shown functional maps is positively ($r > 0$) or

negatively ($r < 0$) associated with discounting for each component map of the k-marker (Choice, LL Amount, Delay).

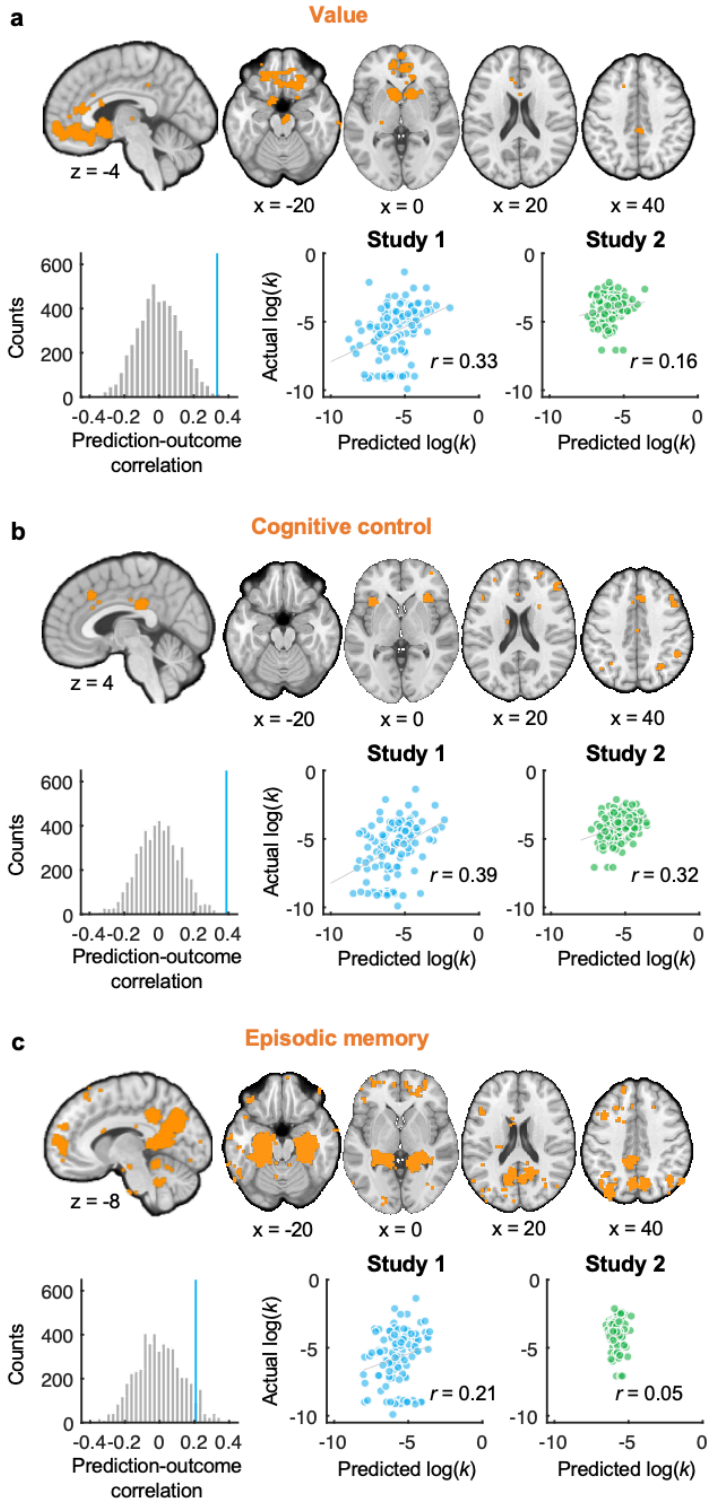

Figure 7. Results for training separate predictive models in three different meta-analytic maps. Term-based meta-analytic maps for **a)** 'value', **b)** 'cognitive control', and **c)** 'episodic memory' were downloaded from Neurosynth (Yarkoni et al., 2011). To obtain

non-overlapping maps (displayed in orange), we masked by excluding voxels that were part of any of the other two maps. We then trained and cross-validated predictive patterns of individual differences in log(k) in the data of Study 1 (blue scatter plots) and further tested the performance of these patterns in Study 2 (green scatter plots). While activity in 'cognitive-control'-related areas led to significant cross-validated prediction in Study 1 and significant transfer to Study 2, such effects were weaker for value or episodic-memory related areas.

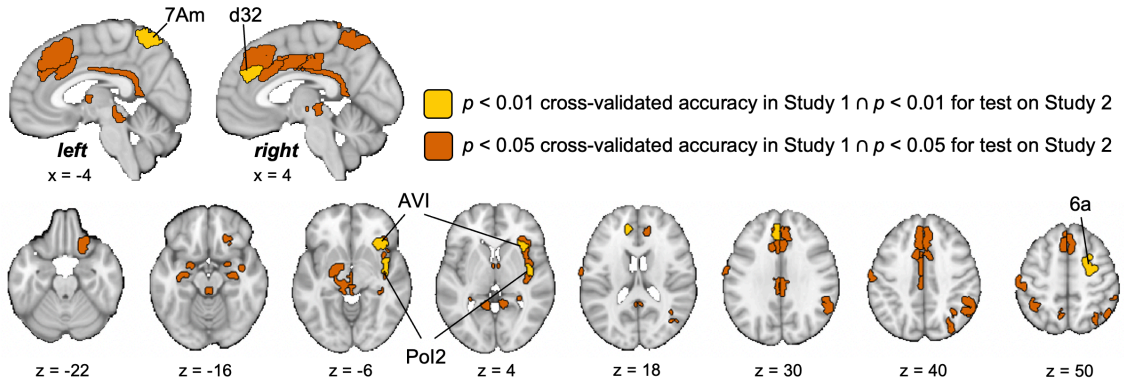

Figure 8. Region of interest (ROI)–based prediction of individual differences in discounting. An established cortical parcellation (Glasser et al., 2016) together with a combination of subcortical parcellations (see atlas available on Github: https://github.com/canlab/Neuroimaging_Pattern_Masks/tree/master/Atlases_and_parcellations/2018_Wager_combined_atlas) was used to test whether functional activity across all three contrasts (Choice, LL -Amount, and Delay) in local brain areas could predict individual log(k)'s. ROIs that resulted in significant cross-validated prediction in Study 1 and significant transfer to Study 2 are shown in yellow (p=0.01 uncorrected for multiple comparisons in both studies) and orange (p=0.05 uncorrected in both studies). They included areas in the mid- and posterior cingulate, dorsomedial prefrontal cortex, several

regions in the right insula, lateral frontoparietal regions, hippocampus, amygdala, thalamus, and brainstem areas.

Extended Data Legends

Figure 1-1. Combination of SS, LL amounts, and delays used in Study 1. Indifference k denotes the discounting rate at which the SS and LL options should be chosen at equal proportions.

Figure 1-2. Combination of SS, LL amounts, and delays used in Study 2. Indifference k denotes the discounting rate at which the SS and LL options should be chosen at equal proportions.

Figure 2-1. Significant positive and negative weights contributing to the k-marker during Choice screen onset (FDR corrected $q < 0.05$ across the whole feature space, i.e., three concatenated gray-matter-masked whole-brain maps, and at least three contingent voxels). In the column 'Atlas label', cortical regions (Ctx) are labeled based on the multimodal cortical parcellation by Glasser et al. (2016), basal ganglia regions based on Pauli et al. (2016), cerebellar regions based on Diedrichsen et al. (2009), and brain stem regions based on a combination of studies (Shen et al., 2013; Bär et al., 2016). The entire combined anatomical atlas is available on Github: https://github.com/canlab/Neuroimaging_Pattern_Masks/tree/master/Atlases_and_parcellations/2018_Wager_combined_atlas. This repository includes multiple atlases and other meta-analytic and multivariate maps. Tools for manipulating and analyzing this and other atlases are in the CANlab Core Tools repository: https://github.com/canlab/CanlabCore.

Figure 2-2. Significant positive and negative weights contributing to the k-marker for the parametric modulation by LL-Amount (FDR corrected $q < 0.05$ across the whole feature

space, i.e., three concatenated gray-matter-masked whole-brain maps, at least three contingent voxels).

Figure 2-3. Significant positive and negative weights contributing to the k-marker for the parametric modulation by Delay (FDR corrected $q < 0.05$ across the whole feature space, i.e., three concatenated gray-matter-masked whole-brain maps, at least three contingent voxels).

Figure 1-1

LL delay (in days)	Display of LL delay	SS amount (in Euro)	LL amount (in Euro)	Indifference *k*
2	In 2 days	5	7.6	0.256
7	In 7 days	5	9.5	0.128
7	In 7 days	5	14.0	0.256
14	In 14 days	5	9.5	0.064
14	In 14 days	5	14.0	0.128
14	In 14 days	5	22.9	0.256
30	In 1 month	5	6.1	0.008
30	In 1 month	5	7.2	0.016
30	In 1 month	5	9.5	0.032
30	In 1 month	5	14.0	0.064
30	In 1 month	5	22.9	0.128
60	In 2 months	5	5.0	0
60	In 2 months	5	5.1	0.00025
60	In 2 months	5	5.2	0.0005
60	In 2 months	5	5.3	0.001
60	In 2 months	5	5.6	0.002
60	In 2 months	5	6.2	0.004
60	In 2 months	5	7.4	0.008
60	In 2 months	5	9.8	0.016
60	In 2 months	5	14.6	0.032
60	In 2 months	5	24.2	0.064
120	In 4 months	5	5.0	0
120	In 4 months	5	5.2	0.00025
120	In 4 months	5	5.3	0.0005
120	In 4 months	5	5.6	0.001
120	In 4 months	5	6.2	0.002
120	In 4 months	5	7.4	0.004

120	In 4 months	5	9.8	0.008
120	In 4 months	5	14.6	0.016
120	In 4 months	5	24.2	0.032
240	In 8 months	5	5.0	0
240	In 8 months	5	5.3	0.00025
240	In 8 months	5	5.6	0.0005
240	In 8 months	5	6.2	0.001
240	In 8 months	5	7.4	0.002
240	In 8 months	5	9.8	0.004
2	In 2 days	10	15.1	0.256
7	In 7 days	10	19.0	0.128
7	In 7 days	10	27.9	0.256
14	In 14 days	10	19.0	0.064
14	In 14 days	10	27.9	0.128
14	In 14 days	10	45.8	0.256
30	In 1 month	10	12.2	0.008
30	In 1 month	10	14.5	0.016
30	In 1 month	10	19.0	0.032
30	In 1 month	10	27.9	0.064
30	In 1 month	10	45.8	0.128
60	In 2 months	10	10.0	0
60	In 2 months	10	10.2	0.00025
60	In 2 months	10	10.3	0.0005
60	In 2 months	10	10.6	0.001
60	In 2 months	10	11.2	0.002
60	In 2 months	10	12.4	0.004
60	In 2 months	10	14.8	0.008
60	In 2 months	10	19.6	0.016
60	In 2 months	10	29.2	0.032
60	In 2 months	10	48.4	0.064
120	In 4 months	10	10.0	0

120	In 4 months	10	10.3	0.00025
120	In 4 months	10	10.6	0.0005
120	In 4 months	10	11.2	0.001
120	In 4 months	10	12.4	0.002
120	In 4 months	10	14.8	0.004
120	In 4 months	10	19.6	0.008
120	In 4 months	10	29.2	0.016
120	In 4 months	10	48.4	0.032
240	In 8 months	10	10.0	0
240	In 8 months	10	10.6	0.00025
240	In 8 months	10	11.2	0.0005
240	In 8 months	10	12.4	0.001
240	In 8 months	10	14.8	0.002
240	In 8 months	10	19.6	0.004
2	In 2 days	20	30.2	0.256
7	In 7 days	20	37.9	0.128
7	In 7 days	20	55.8	0.256
14	In 14 days	20	37.9	0.064
14	In 14 days	20	55.8	0.128
14	In 14 days	20	91.7	0.256
30	In 1 month	20	24.5	0.008
30	In 1 month	20	29.0	0.016
30	In 1 month	20	37.9	0.032
30	In 1 month	20	55.8	0.064
30	In 1 month	20	91.7	0.128
60	In 2 months	20	20.0	0
60	In 2 months	20	20.3	0.00025
60	In 2 months	20	20.6	0.0005
60	In 2 months	20	21.2	0.001
60	In 2 months	20	22.4	0.002
60	In 2 months	20	24.8	0.004

60	In 2 months	20	29.6	0.008
60	In 2 months	20	39.2	0.016
60	In 2 months	20	58.4	0.032
60	In 2 months	20	96.8	0.064
120	In 4 months	20	20.0	0
120	In 4 months	20	20.6	0.00025
120	In 4 months	20	21.2	0.0005
120	In 4 months	20	22.4	0.001
120	In 4 months	20	24.8	0.002
120	In 4 months	20	29.6	0.004
120	In 4 months	20	39.2	0.008
120	In 4 months	20	58.4	0.016
120	In 4 months	20	96.8	0.032
240	In 8 months	20	20.0	0
240	In 8 months	20	21.2	0.00025
240	In 8 months	20	22.4	0.0005
240	In 8 months	20	24.8	0.001
240	In 8 months	20	29.6	0.002
240	In 8 months	20	39.2	0.004

Figure 1-2

LL delay (in days)	Display of LL delay	SS amount (in Dollars)	LL amount (in Dollars)	Indifference *k*
19	19 days	20	43	0.0605
21	21 days	20	22	0.0048
22	22 days	20	54	0.0773
23	23 days	20	30	0.0217
23	23 days	20	54	0.0739
23	23 days	20	67	0.1022
24	24 days	20	77	0.1188
26	26 days	20	45	0.0481
27	27 days	20	41	0.0389
27	27 days	20	22	0.0037
36	36 days	20	30	0.0139
36	36 days	20	58	0.0528
37	37 days	20	63	0.0581
38	38 days	20	43	0.0303
38	38 days	20	24	0.0053
39	39 days	20	80	0.0769
41	41 days	20	75	0.0671
41	41 days	20	50	0.0366
41	41 days	20	67	0.0573
42	42 days	20	23	0.0036
43	43 days	20	34	0.0163
44	44 days	20	73	0.0602
44	44 days	20	29	0.0102
52	52 days	20	74	0.0519
53	53 days	20	58	0.0358
55	55 days	20	58	0.0345
55	55 days	20	41	0.0191

57	57 days	20	32	0.0105
58	58 days	20	81	0.0526
58	58 days	20	29	0.0078
58	58 days	20	66	0.0397
59	59 days	20	50	0.0254
59	59 days	20	28	0.0068
60	60 days	20	75	0.0458
61	61 days	20	23	0.0025
70	70 days	20	25	0.0036
71	71 days	20	66	0.0324
72	72 days	20	58	0.0264
72	72 days	20	45	0.0174
73	73 days	20	58	0.0260
74	74 days	20	67	0.0318
74	74 days	20	25	0.0034
74	74 days	20	82	0.0419
74	74 days	20	32	0.0081
74	74 days	20	31	0.0074
75	75 days	20	29	0.0060
76	76 days	20	31	0.0072
76	76 days	20	71	0.0336
77	77 days	20	23	0.0019
78	78 days	20	33	0.0083
87	87 days	20	24	0.0023
88	88 days	20	71	0.0290
89	89 days	20	57	0.0208
89	89 days	20	24	0.0022
89	89 days	20	64	0.0247
91	91 days	20	27	0.0038
92	92 days	20	79	0.0321
92	92 days	20	44	0.0130

93	93 days	20	56	0.0194
95	95 days	20	72	0.0274
95	95 days	20	39	0.0100
103	103 days	20	33	0.0063
103	103 days	20	67	0.0228
104	104 days	20	39	0.0091
105	105 days	20	83	0.0300
107	107 days	20	45	0.0117
107	107 days	20	55	0.0164
108	108 days	20	25	0.0023
108	108 days	20	78	0.0269
108	108 days	20	70	0.0231
110	110 days	20	23	0.0014
111	111 days	20	32	0.0054
114	114 days	20	36	0.0070
120	120 days	20	43	0.0096
121	121 days	20	74	0.0223
123	123 days	20	28	0.0033
124	124 days	20	60	0.0161
125	125 days	20	24	0.0016
126	126 days	20	54	0.0135
128	128 days	20	48	0.0109
129	129 days	20	50	0.0116
129	129 days	20	85	0.0252
129	129 days	20	78	0.0225
129	129 days	20	41	0.0081
130	130 days	20	27	0.0027
132	132 days	20	28	0.0030
134	134 days	20	23	0.0011
137	137 days	20	65	0.0164
139	139 days	20	24	0.0014

139	139 days	20	52	0.0115
140	140 days	20	36	0.0057
140	140 days	20	49	0.0104
141	141 days	20	25	0.0018
141	141 days	20	61	0.0145
142	142 days	20	77	0.0201
142	142 days	20	27	0.0025
143	143 days	20	44	0.0084
145	145 days	20	66	0.0159
145	145 days	20	80	0.0207
145	145 days	20	42	0.0076
156	156 days	20	65	0.0144
157	157 days	20	45	0.0080
159	159 days	20	40	0.0063
159	159 days	20	65	0.0142
161	161 days	20	77	0.0177
161	161 days	20	76	0.0174
161	161 days	20	39	0.0059
163	163 days	20	55	0.0107
163	163 days	20	28	0.0025
163	163 days	20	33	0.0040
171	171 days	20	35	0.0044
172	172 days	20	49	0.0084
172	172 days	20	69	0.0142
172	172 days	20	56	0.0105
174	174 days	20	41	0.0060
176	176 days	20	71	0.0145
176	176 days	20	34	0.0040
176	176 days	20	23	0.0009
176	176 days	20	25	0.0014
180	180 days	20	62	0.0117

Figure 2-1

Positive weights		Volume	MNI Coordinates			
Name	Atlas label	(voxels)	X	Y	Z	max(z)
Orbitofrontal cortex	Ctx_a47r_L	29	-34	40	-12	4.49
Anterior insula	Ctx_FOP5_R	114	32	24	4	4.45
Midtemporal gyrus	Ctx_PHT_R	18	68	-48	4	4.43
Frontal pole/vmpFC	Ctx_10pp_L	29	-8	60	-12	4.42
Midtemporal gyrus	Ctx_TE1a_R	6	66	-4	-24	4.24
Temporal operculum	Ctx_LBelt_L	32	-42	-28	2	4.21
Other	No_label	9	-2	-28	14	4.13
Visual cortex	Ctx_V2_R	18	20	-100	0	4.04
Orbitofrontal cortex	Ctx_a47r_L	11	-44	38	-12	4.03
Ventrolateral prefrontal cortex	Ctx_45_L	72	-50	28	-2	4.03
Striatum	V_Striatum_R	38	18	26	0	3.99
Striatum	V_Striatum_L	22	0	4	-2	3.96
Orbitofrontal cortex	Ctx_11l_L	13	-18	42	-14	3.95
Retrosplenial cortex	Ctx_RSC_R	15	2	-46	8	3.94
Temporal operculum	Ctx_PoI1_L	20	-38	-4	-16	3.89
Visual cortex	Ctx_V4_R	3	30	-92	22	3.86
Other	No_label	3	66	-54	8	3.84
Visual cortex	Ctx_V3_L	3	-22	-94	24	3.82
Midtemporal gyrus	Ctx_TE1a_L	14	-64	-10	-14	3.79
Amygdala	Ctx_PeEc_R	5	20	6	-26	3.75
Caudate	Cau_L	3	-26	-32	20	3.72
Precentral gyrus	Ctx_4_L	9	-12	-26	70	3.71
Temporal pole/amygdala	Ctx_TGd_R	7	34	12	-24	3.65
Visual cortex	Ctx_V2_L	4	-14	-102	14	3.62
Midtemporal gyrus	Ctx_TGd_R	4	52	4	-26	3.59
Orbitofrontal cortex	Ctx_13l_L	4	-28	28	-14	3.48

Negative weights		Volume				
Name	Atlas label	(voxels)	X	Y	Z	max(z)
Midcingulate cortex	Ctx_24dv_R	58	8	0	36	-5.03
Cerebellum	Cblm_CrusII_L	130	-24	-76	-40	-4.87
Superior frontal gyrus	Ctx_SFL_L	106	-8	10	70	-4.83
Visual cortex	Ctx_ProS_R	79	24	-52	4	-4.81
Inferior parietal lobule	Ctx_PF_L	338	-54	-30	42	-4.75
Precuneus	Ctx_7Am_L	67	-2	-56	60	-4.63
Posterior cingulate cortex	Ctx_23c_R	51	8	-24	40	-4.35
Parietal cortex	Ctx_PGs_R	17	38	-70	52	-4.28
Parahippocampal cortex	Ctx_VMV2_L	7	-32	-50	-6	-4.06
Midcingulate cortex	Ctx_p24pr_L	20	-6	2	36	-4.00
Parahippocampal cortex	Ctx_ProS_L	13	-20	-48	-2	-3.99
Intraparietal sulcus	Ctx_7PC_L	11	-44	-42	60	-3.94
Cerebellum	Cblm_CrusI_R	6	50	-48	-28	-3.88
vmPFC	Ctx_9m_L	8	-8	50	16	-3.87
Cerebellum	Cblm_CrusI_L	6	-46	-64	-42	-3.87
Midcingulate cortex	Ctx_33pr_L	6	-2	22	20	-3.84
Inferior parietal lobule	Ctx_PF_R	13	54	-34	46	-3.83
Inferior frontal cortex	Ctx_6r_L	3	-54	4	16	-3.80
Dorsolateral prefrontal cortex	Ctx_9_46d_R	4	20	48	26	-3.68

Figure 2-2

Positive weights		Volume	MNI Coordinates			
Name	Atlas label	(voxels)	X	Y	Z	max(z)
Medial frontal gyrus	Ctx_8BM_R	386	-2	26	36	5.86
Dorsolateral prefrontal cortex	Ctx_6a_R	199	26	8	52	5.80
Intraparietal Sulcus	Ctx_PFm_R	288	48	-36	52	5.72
Orbitofrontal cortex	Ctx_11l_R	50	16	30	-24	5.55
Inferior parietal lobule	Ctx_PGs_R	298	38	-74	36	5.40
Dorsolateral prefrontal cortex	Ctx_SCEF_L	131	-14	14	52	5.12
Precuneus	Ctx_POS2_R	177	12	-66	38	5.12
Cingulate cortex	Ctx_d32_R	114	10	34	22	4.93
Inferior frontal cortex	Ctx_IFJa_L	134	-44	8	26	4.88
Ventromedial prefrontal cortex	Ctx_p32_L	24	-12	44	4	4.80
Cerebellum	Cblm_IX_R	18	4	-50	-34	4.75
Orbitofrontal cortex	Ctx_11l_L	37	-24	44	-18	4.66
Dorsolateral prefrontal cortex	Ctx_p9_46v_L	67	-46	28	22	4.66
Visual cortex	Ctx_V1_R	29	18	-76	12	4.66
Intraparietal Sulcus	Ctx_AIP_L	24	-38	-44	42	4.61
Inferior parietal lobule	Ctx_IP1_L	58	-32	-72	32	4.57
Posterior cingulate cortex	Ctx_23d_R	56	-2	-28	36	4.56
Anterior insula	Ctx_AVI_L	58	-32	20	2	4.55
Ventrolateral prefrontal cortex	Ctx_a9_46v_R	66	42	46	10	4.47
Ventrolateral prefrontal cortex	Ctx_a9_46v_L	35	-36	44	6	4.40
Ventromedial prefrontal cortex	Ctx_p32_R	47	8	42	0	4.27
Anterior insula	Ctx_AVI_R	16	32	20	2	4.19
Posterior cingulate cortex	Ctx_RSC_R	7	6	-16	32	4.06
Ventromedial prefrontal cortex	Ctx_10r_L	13	-12	38	-8	4.05
Parahippocampal cortex	Ctx_PeEc_R	5	26	-22	-30	4.04
Cerebellum	Cblm_VI_R	11	34	-50	-28	4.02
Thalamus/Pulvinar	Thal_Pulv	10	-12	-32	0	4.00

Medial temporal cortex	Ctx_PreS_R	11	14	-36	0	3.99
Cerebellum	Cblm_CrusI_R	10	40	-40	-38	3.99
Orbitofrontal cortex	Ctx_OFC_L	3	-8	50	-24	3.98
Dorsolateral prefrontal cortex	Ctx_p9_46v_R	9	46	34	24	3.72
Precuneus	Ctx_POS2_R	8	14	-60	24	3.70
Ventrolateral thalamus	Thal_VL	7	-12	-12	14	3.65
Cerebellum	Cblm_VI_L	6	-34	-56	-26	3.61
Precuneus	Ctx_POS2_L	3	-12	-68	36	3.55

Negative weights		Volume				
Name	Atlas label	(voxels)	X	Y	Z	max(z)
Visual cortex	Ctx_V2_L	142	-8	-80	-10	-5.51
Visual cortex	Ctx_V4t_L	70	-42	-82	0	-4.99
Cerebellum	Cblm_CrusI_L	148	-28	-80	-30	-4.93
Cerebellum	Cblm_CrusI_R	64	24	-84	-30	-4.85
Superior frontal cortex	Ctx_SFL_R	47	4	6	68	-4.85
Paracentral lobule	Ctx_4_R	37	6	-30	60	-4.83
Superior parietal lobule	Ctx_7AL_L	158	-20	-40	64	-4.63
Parahippocampal cortex	Ctx_VMV1_R	59	20	-44	-10	-4.60
Visual cortex	Ctx_V3A_L	94	-12	-86	24	-4.51
Superior temporal sulcus	Ctx_STSdp_L	78	-50	-32	-6	-4.49
Cerebellum	Cblm_V_L	16	-22	-34	-30	-4.49
Midcingulate cortex	Ctx_24dv_L	21	-8	-2	40	-4.40
Parahippocampal cortex	Ctx_VMV1_L	32	-18	-60	-8	-4.36
Superior frontal cortex	Ctx_8BL_R	35	2	50	46	-4.28
Visual cortex	Ctx_V4t_R	48	44	-78	-2	-4.23
Visual cortex	Ctx_V3_R	41	16	-72	-8	-4.22
Superior frontal cortex	Ctx_8BL_R	15	4	30	62	-4.20
Superior parietal lobule	Ctx_7AL_R	14	18	-44	70	-4.13
Putamen	Putamen_Pp_R	3	28	-12	10	-4.10

Putamen	Putamen_Pp_L	10	-30	-22	10	-4.06
Superior frontal cortex	Ctx_9a_L	24	-10	62	26	-4.05
Paracentral lobule	Ctx_SCEF_L	11	-8	-6	66	-4.05
Visual cortex	Ctx_V3A_R	31	20	-90	18	-4.00
Frontal pole	Ctx_10d_R	7	12	68	16	-3.90
Temporal pole	Ctx_PeEc_L	4	-28	-4	-34	-3.87
Visual cortex	Ctx_MT_R	9	48	-68	4	-3.83
Superior temporal gyrus	Ctx_PSL_L	17	-56	-36	16	-3.80
Precuneus	Ctx_5L_R	6	12	-48	66	-3.80
Visual cortex	Ctx_V4_R	8	32	-78	-10	-3.79
Superior temporal gyrus	Ctx_A4_L	4	-60	-30	10	-3.70
Temporal pole	Ctx_TE1a_L	4	-52	-6	-32	-3.70
Superior temporal sulcus	Ctx_STV_R	6	50	-42	10	-3.68
Superior temporal gyrus	Ctx_PSL_R	5	54	-32	22	-3.56

Figure 2-3

Positive weights		Volume	MNI Coordinates			
Name	Atlas label	(voxels)	X	Y	Z	max(z)
Visual cortex	Ctx_V3A_R	131	12	-86	20	5.30
Ventromedial prefrontal cortex	Ctx_10v_R	160	2	42	-20	5.14
Precuneus	Ctx_PCV_L	102	-10	-54	46	4.75
Superior temporal sulcus	Ctx_STSdp_L	63	-54	-34	4	4.71
Superior temporal gyrus	Ctx_TA2_R	59	52	-8	-2	4.66
Precentral gyrus	Ctx_3b_L	214	-34	-26	62	4.62
Angular gyrus	Ctx_PGi_R	27	40	-60	22	4.61
Ventromedial prefrontal cortex	Ctx_9m_R	37	16	48	6	4.58
Putamen	Putamen_Pp_L	35	-32	-14	2	4.43
Caudate	Cau_L	36	-22	22	2	4.35
Superior temporal gyrus	Ctx_TPOJ1_R	29	50	-30	8	4.34
Angular gyrus	Ctx_PGi_L	43	-48	-54	22	4.34
Precentral gyrus	Ctx_4_L	5	-32	-16	44	4.33
Cingulate sulcus	Ctx_24dd_L	49	-6	-10	48	4.29
Subgenual cingulate cortex	Ctx_s32_L	17	-10	26	-12	4.24
Paracentral lobule	Ctx_5L_R	28	10	-40	62	4.16
Midcingulate cortex	Ctx_24dv_R	9	10	-4	44	4.15
Cerebellum	Cblm_CrusII_L	3	-12	-84	-44	4.04
Caudate	Cau_R	7	6	26	-4	3.99
Superior frontal gyrus	Ctx_9m_R	21	4	56	38	3.97
Midtemporal gyrus	Ctx_MT_R	9	46	-68	12	3.96
Visual cortex	Ctx_V1_L	14	-14	-82	-4	3.94
Cerebellum	Cblm_CrusII_R	7	28	-84	-44	3.93
Posterior insula/temporal operculum	Ctx_52_R	16	40	-22	-2	3.91
Superior temporal sulcus	Ctx_A5_L	8	-58	2	-10	3.90
Paracentral lobule	Ctx_5mv_R	4	18	-32	44	3.83
Cerebellum	Cblm_CrusI_R	10	40	-74	-34	3.82

Midtemporal gyrus	Ctx_A5_L	4	-62	-12	-10	3.80
Superior parietal lobule	No_label	4	-22	-44	50	3.78
Paracentral lobule	Ctx_5m_L	11	-10	-44	64	3.77
Paracentral lobule	Ctx_5mv_R	7	16	-24	44	3.72
Inferior frontal cortex	Ctx_45_L	5	-54	26	14	3.72
Precentral gyrus	Ctx_6d_L	3	-26	-18	62	3.72
Superior parietal lobule	Ctx_7Am_L	5	-4	-66	62	3.70
Visual cortex	Ctx_V2_L	8	-6	-86	18	3.69
Visual cortex	Ctx_IP0_R	6	30	-70	22	3.68
Caudate	Cau_L	4	-18	8	18	3.68
Posterior cingulate cortex	Ctx_24dd_R	7	10	-20	44	3.66
Superior parietal lobule	Ctx_2_L	3	-18	-38	60	3.63
Superior temporal sulcus	Ctx_STV_R	3	58	-34	8	3.57

Negative weights		Volume				
Name	Atlas label	(voxels)	X	Y	Z	max(z)
Dorsolateral prefrontal cortex	Ctx_a9_46v_L	76	-40	50	14	-5.20
Brain stem	Bstem_Ponscd	54	2	-28	-36	-4.78
Intraparietal sulcus	Ctx_7PC_L	34	-40	-46	48	-4.70
Dorsolateral prefrontal cortex	Ctx_8C_R	26	40	12	30	-4.57
Brain stem	Bstem_Ponscd_L	69	-12	-38	-36	-4.54
Paracentral lobule	Ctx_4_R	12	6	-30	78	-4.41
Inferior parietal lobule	Ctx_PFm_R	23	54	-44	52	-4.39
Cerebellum	Cblm_Dentate_R	39	18	-42	-36	-4.25
Cerebellum	Cblm_IX_L	51	-6	-54	-36	-4.23
Medial frontal gyrus	Ctx_8BM_R	45	0	22	42	-4.17
Orbitofrontal cortex	Ctx_a10p_R	5	22	58	-10	-4.16
Visual cortex	Ctx_V4_R	19	30	-86	-10	-4.11
Paracentral lobule	Ctx_SFL_R	10	4	-2	76	-4.10
Thalamus	Thal_Pulv	13	-4	-30	4	-4.08
Orbitofrontal cortex	Ctx_11l_R	17	22	32	-18	-4.07

Visual cortex	Ctx_LO2_L	3	-46	-82	-6	-4.07
Anterior insula/frontal operculum	Ctx_AVI_R	3	36	26	-4	-4.06
Dorsolateral prefrontal cortex	Ctx_p9_46v_R	52	44	36	16	-3.99
Cerebellum	Cblm_CrusII_R	3	8	-86	-28	-3.92
Frontal pole	Ctx_a10p_R	9	28	66	-6	-3.85
Thalamus	Thal_Pulv	19	6	-26	8	-3.85
Orbitofrontal cortex	Ctx_pOFC_R	8	16	10	-16	-3.84
Midcingulate cortex	Ctx_a32pr_L	4	-8	34	24	-3.84
Visual cortex	Ctx_V4_L	10	-34	-90	-6	-3.80
Frontal pole	Ctx_a10p_L	3	-20	60	-10	-3.80
Visual cortex	Ctx_V3CD_L	9	-44	-86	12	-3.79
Superior parietal lobule	No_label	3	28	-38	76	-3.79
Posterior cingulate cortex	Ctx_31a_L	9	0	-32	44	-3.74
Inferior parietal lobule	Ctx_PFm_L	4	-50	-48	52	-3.69
Frontal pole	Ctx_p10p_L	3	-30	66	0	-3.65
Visual cortex	Ctx_VVC_R	4	30	-62	-14	-3.63
Nucleus accumbens	NAC_L	6	-10	4	-18	-3.57
Nucleus accumbens	NAC_L	3	-8	12	-10	-3.52